Currents in the Kaštela Bay: empirical analysis and results of a numerical model

Gordana BEG PAKLAR, Mira ZORE-ARMANDA and Vlado DADIĆ

Institute of Oceanography and Fisheries, P.O.Box 500, 21000 Split, Croatia

Basic statistical analysis of all available current data from the Kaštela Bay for a period between 1953 and 1990 shows the importance of the sirocco *wind in generating the circulation of the Bay. Strong episodes of* sirocco *reverse the estuarine circulation in the Bay inlet. During sirocco episodes current polarisation in the east-west direction is observed, with a downwind current in the surface layer and the compensatory current in the deeper layers. In the Bay interior sirocco-induced surface currents turn to the right of the wind direction under the influence of the CORIOLIS force. During strong wind periods the mean current speeds in the Bay interior are almost half of those in the Bay inlet, pointing to the importance of the wind-induced transports from the adjacent Brač Channel.*

Numerically obtained basin-wide cyclonic circulation during bora *wind is in agreement with the conclusions of the salinity measurement analysis. Numerical results show the formation of several cyclonic and anticyclonic gyres during* sirocco, *so at least in some parts of the basin theoretical results and empirical findings stemming from the salinity distribution are in agreement. Comparison of direct current measurements with the results of the numerical model shows good agreement during* sirocco *episodes, whereas the agreement is lower during* bora. *Proper prediction of the wind-induced currents demands detailed knowledge of the wind stress magnitude and direction above the Kaštela Bay and of the density distribution in the sea.*

Key words: Kaštela Bay, currents, *bora, sirocco*

INTRODUCTION

The Kaštela Bay is a small semi-enclosed basin on the eastern Adriatic coast, with a total area of 61 km² and a mean depth of 23 m (Fig. 1). During the last few decades, several sets of current measurements were performed in the Kaštela Bay in order to study its circulation. The intention of this article is three-fold: to review the results of the various current data sets collected between 1953 and 1990, to compare them to numerical model results, and to stress a need for new field experiments based on the empirical and theoretical findings.

The first current measurements in the Kaštela Bay during 1953 and 1954 were performed from anchored ships under calm weather conditions, and resulted in determination of the seasonal distribution of surface currents (ZORE-ARMANDA *et al.*, 1969). Results of two similar current measurements in the 1970's showed that during calm weather the Kaštela Bay behaves as a typical dilution basin, with an outgoing current in the surface layer and an

incoming current in the deeper layers (ZORE-ARMANDA *et al.*, 1974)

During the 1980's currents in the Kaštela Bay were measured with moored AANDERAA currentmeters that can be easily deployed in shallow coastal areas, and provide a long time-series of current data. Between 1980 and 1990 seven current measurements were performed, during which currents were measured in different seasons and at various stations and depths. A typical duration of the obtained time-series was two months. The introduction of this new technology greatly improved the knowledge of the Kaštela Bay current field and understanding of its dynamics. Due to the long duration of these measurements, spectral analysis of the current time-series showed the importance of the wind-induced currents, connected with the synoptic atmospheric disturbances on the time scales of several days (GAČIĆ, 1982). The empirical orthogonal function analysis showed that 70% of the total variance could be explained in terms of the local wind forcing (GAČIĆ *et al.*, 1987). This new measurement technique employing moored currentmeters allowed analysis of the characteristics of the Kaštela Bay current field during the strong wind events (BEG PAKLAR and GAČIĆ, 1997), which was not possible from the anchored ships data in the past.

Basic statistical analysis of all available current data is performed in this paper. Due to the great importance of the wind forcing on the Kaštela Bay current field as deduced from the analysis of the hydrographic (ZORE-ARMAN-DA, 1980) and direct current measurements (GAČIĆ, 1982; GAČIĆ *et al.*, 1987; BEG PAK-LAR and GAČIĆ, 1997), particular attention has been paid to the wind-induced currents. Two most frequent winds are northeastern and southeastern winds called *bora* and *sirocco*, respectively. In the studied area they blow with a mean speed of 10 ms^{-1} (PENZAR, 1977). The wind-induced currents were simulated with Princeton Ocean Model (POM) (BLUMBERG and MELLOR, 1987) and the numerical model results were compared to the results of the empirical analysis. The numerical model

involves a complete three-dimensional thermodynamics with BOUSSINESQ and hydrostatic approximations. The second-order turbulence closure model "Level 2 1/2" (MELLOR and YAMADA, 1982), providing vertical eddy viscosity and diffusivity coefficients, is embedded in the main model.

Wind-induced currents in the Kaštela Bay have been until now simulated by two numerical models: the HEAPS spectral three-dimensional model (ORLIĆ *et al.*, 1989) and the non-linear three-dimensional multilevel model (BONE *et al.*, 1992; BONE, 1993). Differences between the simulated values of wind-induced currents as obtained by POM and by the other two numerical models, are due to a differently defined dynamical background, different numerical schemes and different parameterisation used in the models.

This paper is organised as follows: the following section contains a description of the current measurements and the results of statistical analysis. Numerical model results are given in the next section, together with their comparison with empirical data. The discussion with main conclusions is given in the last section. A description of the employed numerical model is given in the ANNEX.

CURRENT MEASUREMENTS AND THEIR RESULTS

Empirical analyses were performed on the basis of the following data sets (Fig. 1):

1. 1953-1954 currents were measured with a direct reading EKMAN currentmeter at seven stations, twice a month (ZORE-ARMANDA *et al.*, 1969), with a maximal duration of 24 hours.

2. 1972-1973 twenty-four hour time-series were obtained using ALEKSEJEV currentmeters at five stations (ZORE-ARMANDA *et al.*, 1974).

3. 1975-1976 six, twelve and twenty-four hour time-series were obtained using direct reading EKMAN currentmeter at seven stations in the Vranjic basin. Drift-cards were
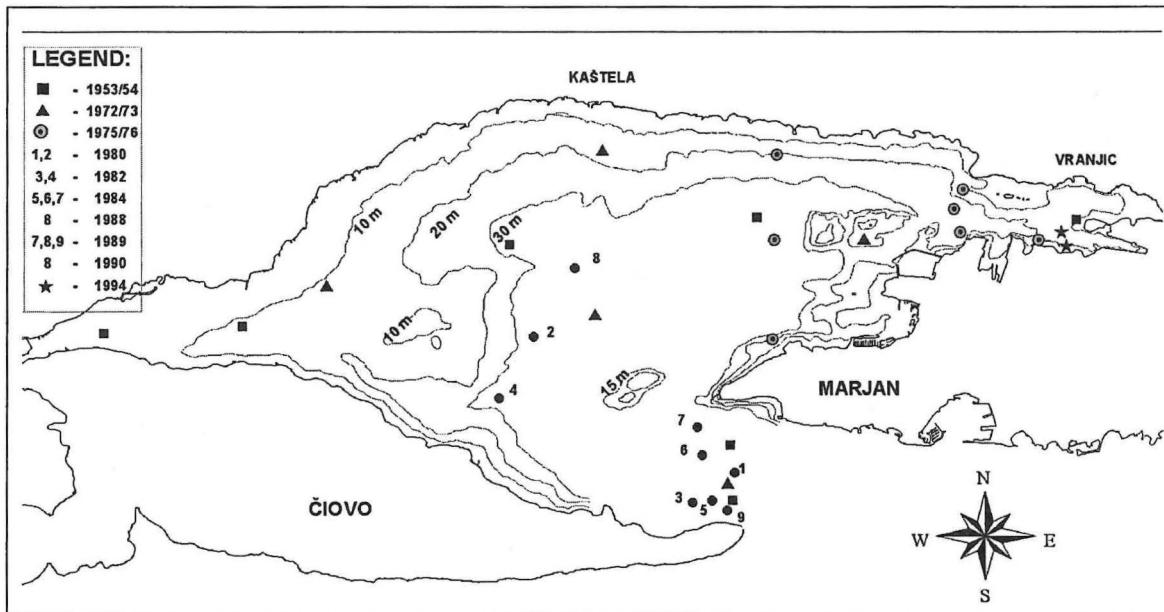
Fig. 1. The chart of the Kaštela Bay with the locations of the current measurement points. Currentmeter moorings from the period 1980-1990 are marked with numbers (1-9). Locations of the stations in the 1953 - 54 period are marked with a rectangle (■), those from the 1972 - 73 period with a triangle (▲) and the stations from the 1975 - 76 period with a circle (☉)

simultaneously deployed from the same stations (ZORE-ARMANDA *et al.*, 1976).

4. 22nd September - 7th November 1980 currents were measured with AANDERAA RCM-4 currentmeters at two stations. The first one was in the Kaštela Bay inlet, and the second in the basin interior near its southern coast. At both stations the currents were measured at 10 and 30 m depths. The currentmeter in the Bay inlet at 10 m stopped recording after several days, due to malfunction (GAČIĆ, 1982).

5. 22nd September - 9th November 1982 currents were measured with AANDERAA currentmeters at two stations whose positions were similar to the positions of the stations during the 1980 measurement. The first station was in the Bay inlet and currents were measured at four levels (8, 20, 30 and 40 m), whereas the second one was in the basin interior and currents were measured at three levels (8, 15 and 22 m) (GAČIĆ *et al.*, 1987).

6. 15th January - 5th March 1984 currents were measured with AANDERAA currentmeters in the intermediate layer at three stations in the Bay inlet. Two of the time-series were

only a few days long due to instrument malfunction (BEG, 1992).

7. 28th April - 7th July and 11th August - 20th October 1988 currents were measured with AANDERAA currentmeters at the central Bay station, first at three levels (5, 20 and 30 m), and than at two levels (5 and 30 m) (BEG, 1992).

8. 3rd March - 12th May 1989 currents were measured with AANDERAA currentmeters at three stations. Two stations were placed at the Bay inlet, whereas the third one was in the Bay interior. Measurements were performed at 5 and 30 m at all stations (GAČIĆ *et al.*, 1991).

9. 16th October - 19th December 1990 currents were measured with AANDERAA currentmeters at the Bay interior station at three levels (5, 20 and 30 m) (BEG, 1992).

Hourly wind data from the nearby meteorological station Split-Marjan were used in the analysis of the wind influence on the Kaštela Bay current field.

In the following statistical analysis the current measurement data obtained during the 1953 - 1975 period are not included. The maximal

duration of the measurements was only 24 hours, and therefore the amount of data is several orders of magnitude lower than the amounts obtained in the 1980's. In the formal statistical analysis old data would be completely covered with new one. Additionally, the current data before and after 1980 were obtained under different conditions and with different technology and they obviously present, in many ways, a different picture. One of our aims is to stress the differences between the two data sets, although we realise that the difference is not statistically significant because of large discrepancies in the data amounts.

Basic statistical analysis of the current data obtained in the 1980 - 1990 period has shown that the mean vector velocity in the surface layer is between 0.7 and 8.3 cms^{-1} (Table 1).

Table 1. Basic statistical analysis of the currents in the Kaštela Bay during the period 1980- 1990

station	depth (m)	year	duration of the measurements	mean vector speed (cms^{-1})	mean direction	mean scalar speed (cms^{-1})
1	30	1980	22.9-24.10.	2.8	357.8 N	17.1
2	10	1980	22.9-7.11.	8.3	311.2 NW	14.1
	30	1980	22.9-7.11.	7.2	21.8 N	16.9
3	8	1982	22.9-4.11.	2.6	279.7 N	5.6
	20	1982	22.9-4.11.	2.7	291 W	6.5
	30	1982	22.9-4.11.	1.7	322.7 NW	6.4
	40	1982	22.9-4.11.	0.7	121.3 SE	5.8
4	8	1982	22.9-28.10.	2.9	331 NW	4.4
	15	1982	22.9-28.10.	2.1	346 N	3.6
	22	1982	22.9-28.10.	0.7	353 N	2.9
5	20	1984	12.1-24.1	4.6	280 N	6.0
6	20	1984	12.1-5.3.	3.0	116 SE	8.0
7	24	1984	12.1-26.1.	1.5	44 NE	7.9
	5	1989	3.3-13.5.	4.0	274 W	7.0
	30	1989	3.3-30.3.	5.5	317 NW	6.0
8	5	1988	28.4-6.7.	6.1	33 NE	13.0
	20	1988	28.4-7.7.	3.2	65 NE	5.1
	30	1988	28.4-7.7.	2.6	76 E	4.8
	5	1988	11.8-14.10.	1.7	13 N	5.7
	30	1988	11.8-20.10.	2.7	77 E	5.3
	5	1989	7.3-8.5.	0.7	71 E	6.0
	30	1989	7.3-13.4.	2.3	65 NE	4.2
	5	1990	16.10-16.12.	1.2	5 N	5.4
	20	1990	16.10-19.12.	3.5	53 NE	5.5
	30	1990	16.10-19.12.	1.9	56 NE	3.0
9	5	1989	3.3-12.5.	3.8	123 SE	7.4
	30	1989	3.3-12.5.	5.4	75 E	7.2

The lowest values were obtained during spring, whereas the strongest currents occurred in autumn, in agreement with earlier results (ZORE-ARMANDA, 1980). Corresponding scalar mean in the surface layer is between 5 and 14 cms^{-1} (Table 1). In the whole water column, the strongest currents are toward northeastern direction, followed by the eastern and western currents (Table 2).

Table 2. Current speeds of eight directions (octans) from the mesurements 1980- 1990

station	depth (m)	year	N	NE	E	SE	S	SE	W	NW
1	30	1980	19.9	24.0	18.7	21.8	28.3	17.5	13.5	13.5
	10	1980	12.7	13.7	15.6	15.5	16.2	15.6	13.7	14.4
2	30	1980	14.5	21.2	21.6	12.0	23.7	21.3	12.4	10.9
	8	1982	3.8	3.7	6.1	5.8	3.5	4.0	6.8	6.2
	20	1982	3.9	4.2	8.4	7.9	3.9	3.7	6.8	6.9
3	30	1982	3.2	3.7	8.8	7.0	3.2	3.2	7.0	6.6
	40	1982	2.6	2.6	10.6	6.2	2.3	2.5	5.7	5.2
	8	1982	4.2	3.2	3.2	2.7	3.7	3.9	4.4	5.5
4	15	1982	4.3	3.9	2.8	2.0	2.3	2.4	2.6	4.4
	22	1982	3.4	3.5	3.0	2.5	2.0	2.2	2.8	3.4
5	20	1984	3.0	3.4	4.4	3.8	4.1	4.9	7.0	5.6
6	20	1984	6.2	5.3	9.8	8.8	5.9	6.9	7.3	7.1
	24	1984	6.7	12.7	6.3	8.6	9.0	9.3	10.4	7.2
7	5	1989	3.4	2.5	2.6	7.6	5.0	3.1	8.8	8.5
	30	1989	3.1	3.5	6.2	7.5	5.8	7.3	10.4	6.3
	5	1988	20.2	12.9	10.1	10.2	8.5	7.5	8.3	12.2
	20	1988	5.1	6.8	4.9	3.5	3.7	4.7	4.7	3.8
	30	1988	4.0	5.8	4.7	6.0	3.8	2.9	3.9	2.6
	5	1988	9.7	6.1	3.0	3.7	4.6	5.4	4.9	9.1
8	30	1988	3.2	8.9	4.4	5.1	3.3	2.9	3.5	2.4
	5	1989	7.9	5.0	5.3	4.8	4.7	6.3	8.2	8.0
	30	1989	3.1	4.8	4.0	3.9	3.5	3.2	3.3	5.1
	5	1990	7.5	4.4	3.8	4.5	4.5	4.8	7.5	6.1
	20	1990	5.6	6.1	5.2	5.9	4.7	3.3	4.4	4.8
	30	1990	3.4	5.8	2.7	4.3	4.3	2.0	2.9	1.9
9	5	1989	4.2	4.0	7.3	8.0	6.1	3.8	7.4	10.0
	30	1989	1.9	5.3	9.2	2.5	2.0	2.1	4.5	4.8

The strongest northeastern currents were recorded in the central part of the Bay in the intermediate and bottom layers, which is the current direction that occurs there during *sirocco* wind episodes. Strong eastern and western currents are obtained in the Bay inlet also during *sirocco* episodes. Therefore, *sirocco* is an important generating mechanism for the cur-

rents in the Bay. The importance of the *sirocco*-induced currents is pronounced due to basin geometry, with Bay inlet exposed to it. Results in Table 3 show that northern direction is the most frequent at the stations in the Bay interior, and it is followed by northeastern and northwestern directions. Northwestern, eastern and western directions are the most frequent in the Bay inlet.

Table 3. The frequency of current dirrections (octans) in percentages for the period 1980 -1990

station	depth (m)	year	N	NE	E	SE	S	SE	W	NW
1	30	1980	19.9	24.0	18.7	21.8	28.3	17.5	13.5	13.5
	10	1980	12.7	13.7	15.6	15.5	16.2	15.6	13.7	14.4
2	30	1980	14.5	21.2	21.6	12.0	23.7	21.3	12.4	10.9
	8	1982	3.8	3.7	6.1	5.8	3.5	4.0	6.8	6.2
	20	1982	3.9	4.2	8.4	7.9	3.9	3.7	6.8	6.9
3	30	1982	3.2	3.7	8.8	7.0	3.2	3.2	7.0	6.6
	40	1982	2.6	2.6	10.6	6.2	2.3	2.5	5.7	5.2
	8	1982	4.2	3.2	3.2	2.7	3.7	3.9	4.4	5.5
4	15	1982	4.3	3.9	2.8	2.0	2.3	2.4	2.6	4.4
	22	1982	3.4	3.5	3.0	2.5	2.0	2.2	2.8	3.4
5	20	1984	3.0	3.4	4.4	3.8	4.1	4.9	7.0	5.6
6	20	1984	6.2	5.3	9.8	8.8	5.9	6.9	7.3	7.1
	24	1984	6.7	12.7	6.3	8.6	9.0	9.3	10.4	7.2
7	5	1989	3.4	2.5	2.6	7.6	5.0	3.1	8.8	8.5
	30	1989	3.1	3.5	6.2	7.5	5.8	7.3	10.4	6.3
	5	1988	20.2	12.9	10.1	10.2	8.5	7.5	8.3	12.2
	20	1988	5.1	6.8	4.9	3.5	3.7	4.7	4.7	3.8
	30	1988	4.0	5.8	4.7	6.0	3.8	2.9	3.9	2.6
	5	1988	9.7	6.1	3.0	3.7	4.6	5.4	4.9	9.1
8	30	1988	3.2	8.9	4.4	5.1	3.3	2.9	3.5	2.4
	5	1989	7.9	5.0	5.3	4.8	4.7	6.3	8.2	8.0
	30	1989	3.1	4.8	4.0	3.9	3.5	3.2	3.3	5.1
	5	1990	7.5	4.4	3.8	4.5	4.5	4.8	7.5	6.1
	20	1990	5.6	6.1	5.2	5.9	4.7	3.3	4.4	4.8
	30	1990	3.4	5.8	2.7	4.3	4.3	2.0	2.9	1.9
9	5	1989	4.2	4.0	7.3	8.0	6.1	3.8	7.4	10.0
	30	1989	1.9	5.3	9.2	2.5	2.0	2.1	4.5	4.8

Currents in the Bay inlet

The current system in the Kaštela Bay inlet is of great importance for the Bay dynamics. From the hydrographic point of view, the Kaštela Bay is a dilution basin. River Jadro, with a mean annual runoff of $10\ m^3 s^{-1}$, and several subsurface springs, occasionally very active, discharge into the Bay lowering its salinity. Therefore salinity in the Kaštela Bay is considerably lower than that of the sea in the adjacent Brač Channel.

The empirical and theoretical considerations of the flow in the Bay inlet were simplified by grouping data from all the stations. The 1972 - 1973 current measurements, performed with direct reading EKMAN currentmeters, and the corresponding hydrographic analyses, showed that the low-salinity water flows in the surface layer and leaves the basin, whereas a compensating incoming current of saltier water flows in the bottom layer (ZORE-ARMANDA, 1980) (Fig. 2 a, b).

Measurements were performed from an anchored ship during calm weather, which means that in the situations without wind Kaštela Bay behaves as a typical dilution basin. By considering the latest current time-series obtained by moored currentmeters, rather different current rose has been constructed (Fig. 2 c, d).
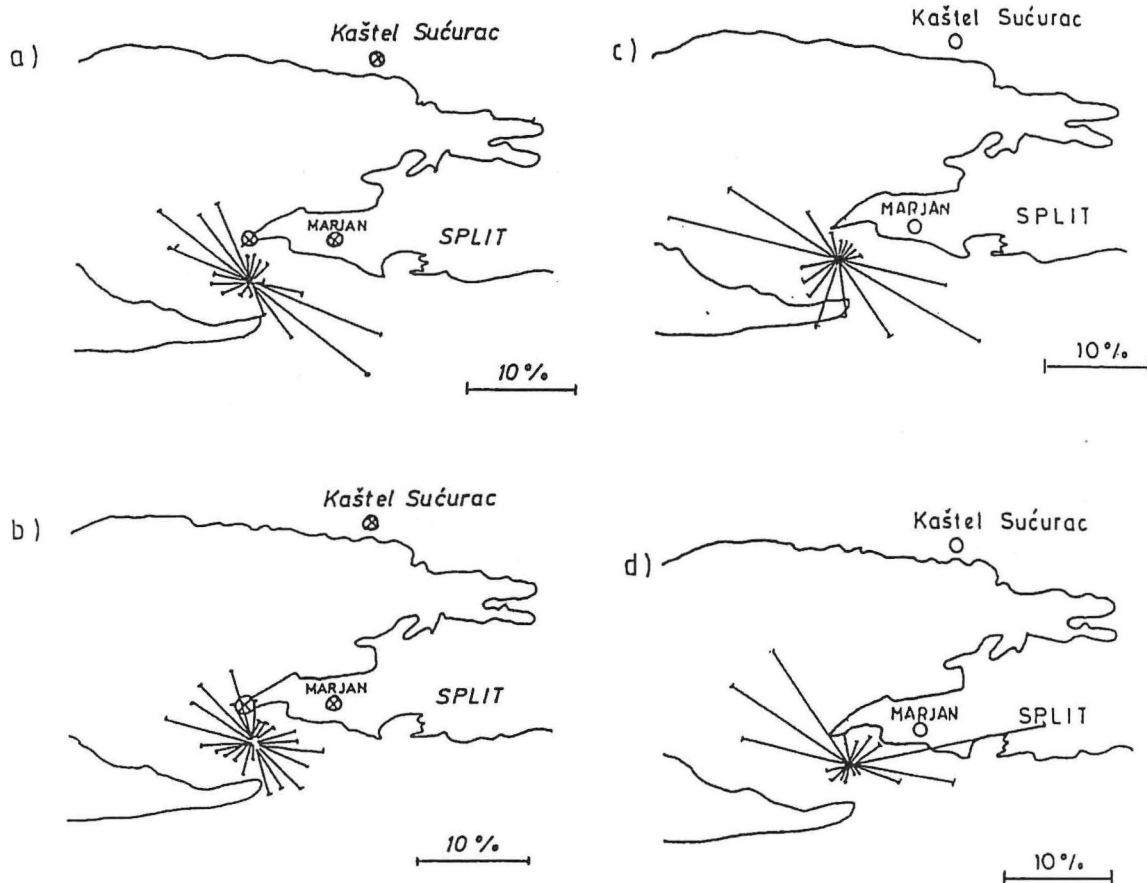
Fig 2. Current roses constructed for the Kaštela Bay inlet according to the occurrence frequency of the directions at the surface (a, c) and at the bottom (b, d) layers for the periods 1953-1975 (left) and 1980-1990 (right). Small circles mark meteorological stations whose data were used
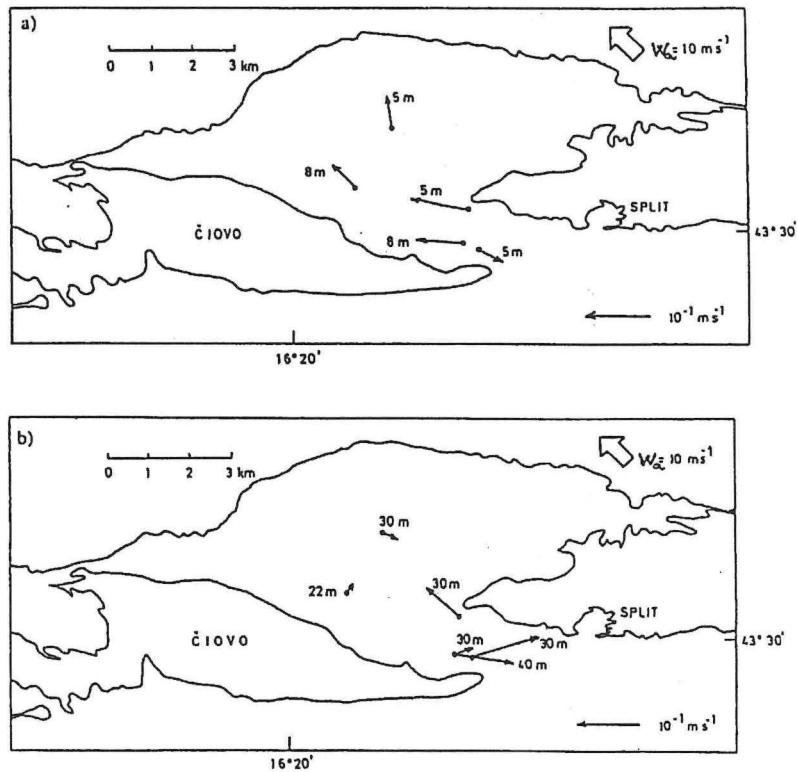
Fig. 3. Spatial distribution of the averaged current vectors during sirocco episodes, with filtered speeds (24m214) exceeding 5 ms⁻¹, at both the surface (a) and the bottom (b) layers. The average wind speed during episodes with wind speed exceeding 5 ms⁻¹ was 10 ms⁻¹. The currentmeter level is denoted next to the current vector

It shows that incoming currents prevail at the surface. Although incoming flow prevails at the bottom one of the outgoing direction is the most frequent. During *sirocco* wind episodes current system with incoming drift current in the surface layer and outgoing compensating current in the bottom layer is obtained from early hydrographic considerations (ZORE-ARMANDA, 1980), as well as from the latest direct current measurements (Fig. 3). Since the mean vectors coincide with vectors obtained during *sirocco* episodes, the dominant influence of the *sirocco*-induced currents on the Bay inlet dynamic is obvious. Therefore, during strong *sirocco* events gravitational circulation is completely reversed, which agrees with the analytical results for the estuarine circulation under the wind influence, obtained by PRITCHARD (1954; 1956). Both the wind-induced and the gravitational currents are polarised in the east-west direction due to the orientation of the inlet.

The currentmeter data obtained during the 1980 - 1990 period with AANDERAA current-meters showed that in most cases of strong *sirocco* events an incoming current in the surface layer is formed. However an outgoing current was recorded along the northern coast (Marjan) at the end of September 1982 (GAČIĆ *et al.*, 1987) and along the southern coast (Čiovo Island) in April 1989, both during *sirocco* episodes (GAČIĆ *et al.*, 1991) (Fig. 3). During both events the outgoing current was compensating the incoming current flowing along the opposite inlet coast. Since the Bay salinity was the lowest in April and the pycnocline was still well pronounced during September, it can be concluded that horizontal compensation in the Bay inlet occurs in stratified period. The obtained horizontal current compensation in the Bay inlet during periods with stratified water is a consequence of the superposition of two oppositely directed current systems: the wind induced-currents and the
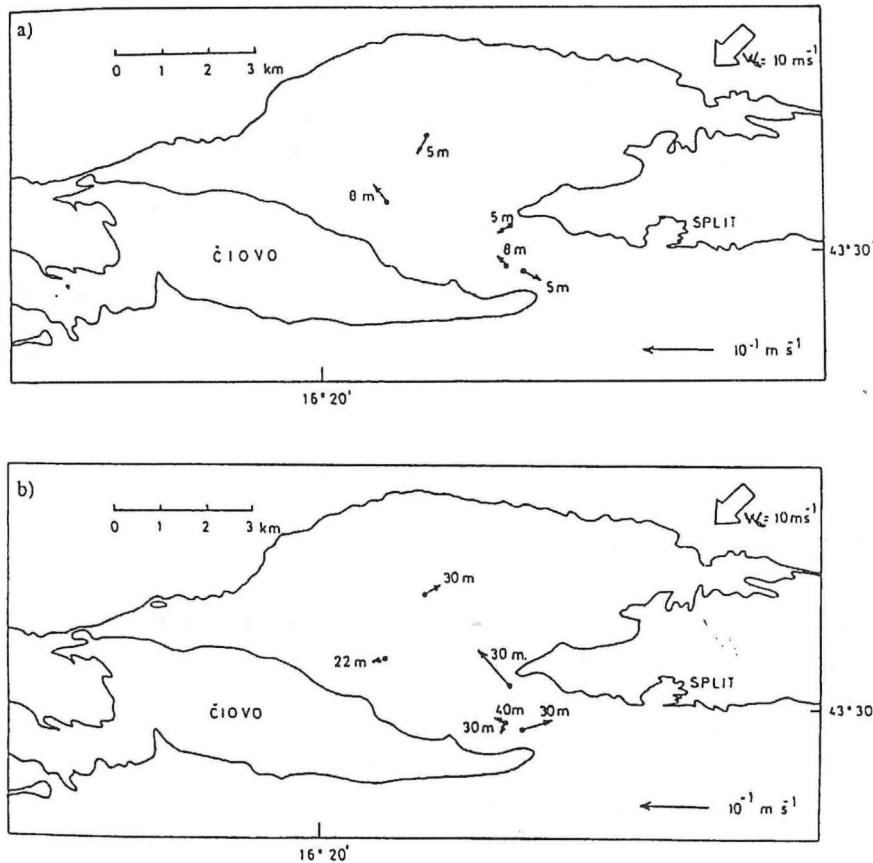
Fig. 4. Spatial distribution of the averaged current vectors during bora episodes, with filtered speeds (24m214) exceeding 5 ms⁻¹, at the surface (a) and the bottom (b) layer. The average wind speed during episodes with wind speed exceeding 5 ms⁻¹ was 10 ms⁻¹. The currentmeter level is denoted next to the current vector

gravitational current system. Currents in the Bay inlet depend on the relative strength of the two current systems, which results in a considerable variability of the currents in the surface and the lower layers. The horizontal compensation in the Bay inlet during a stratified period is also favoured by the fact that the pycnocline prevents the momentum exchange between the surface and the lower layers. Since no current data pertaining to the summer condition are presently available, we can only assume that in the Kaštela Bay inlet gravitational circulation dominates during summer months. Moreover, it is expected that a low frequency of strong synoptic winds during summer would favour prevalence of the gravitational circulation.

Bora is a spatially variable wind, and above the Kaštela Bay inlet its direction is modified by a complex orography of the Bay surroundings.

Currentmeter data indicate that the water exchange between the Bay and the adjacent Brač channel is much less intensive during *bora* than during *sirocco* (Fig. 4). Prevalence of a weak outgoing current in the surface layer, in conjunction with an incoming current in the bottom layer, is deduced from hydrographic considerations (ZORE-ARMANDA, 1980) and direct current measurements (BEG PAKLAR and GAČIĆ, 1997). It is well known that *bora* along the eastern Adriatic coast induces an offshore current with a corresponding upwelling (ZORE-ARMANDA, 1986; BERGAMASCO and GAČIĆ, 1996), and the same situation probably occurs in the Kaštela Bay.

The mean current speed in the surface layer in the Kaštela Bay inlet is 7.6 cms⁻¹, in the intermediate layer 6.9 cms⁻¹ and in the bottom layer 8.1 cms⁻¹ (Table 4). The vertical distribution of

Table 4. Statistics for the bay inlet and bay interior in the surface, intermediate and bottom layer

	mean vector speed	mean direction	mean scalar speed	N component (v)	E component (u)	number of data
inlet (surface)	1.47	188.53	7.65	-0.22	-1.46	4494
inlet (intermed)	0.29	336.58	6.91	-0.11	0.26	2781
inlet (bottom)	1.97	50.85	8.13	1.53	1.25	5012
interior (surface)	2.12	100.91	6.47	2.08	-0.40	8075
interior (intermed)	2.78	39.31	4.82	1.76	2.15	4080
interior (bottom)	2.61	38.91	5.67	1.64	2.03	7710

the mean currents indicates that currents in the bottom layer generally compensate the surface currents. This negative correlation between the wind and the currents in the bottom layer at the majority of the inlet stations during strong winds indicates that two-layer model can be applied to the inlet flow (Table 5). The results derived from two simple analytical models (RATTRAY and HANSEN, 1965; WANG, 1979) show that two-layer structure in small semi-enclosed basins can be obtained by taking into account the pressure gradient force and a vertical turbulent momentum exchange. Regression analysis from BEG PAKLAR and GAČIĆ (1997) paper with the assumption of viscous balance, results in unacceptable high values for the bottom friction coefficient. This points to the conclusion that forces besides the viscous ones affect the flow in the Bay inlet in a direction opposite to the wind. This particularly applies to the pressure gradient force.

The mean speed of the eastern current component in the Bay inlet, according to all available data, is 1.45 cms⁻¹ in the surface layer, 0.26 cms⁻¹ in the intermediate layer and 1.2 cms⁻¹ in the bottom layer (Table 4). According to these values the flushing period is 55 days. During *sirocco* wind with speed of 10 ms⁻¹ flushing period become substantially shorter with value of 6 days (BEG PAKLAR and GAČIĆ, 1997).

Currents in the Bay interior

According to earlier measurements during calm periods, the currents in the Bay interior are weaker than in the inlet (ZORE-ARMANDA, 1980). Upon entering the Bay the surface layer water takes the direction along either of the coasts. An earlier statistical analysis (GAČIĆ and SMIRČIĆ, 1973) has shown that data from the stations at the Bay inlet coincided better with data from the stations close to the inlet coasts than with data collected at stations in the central part of the Bay. These results indicate a presence of a closed circulation in the Bay.

The mean current vector in the surface layer, according to all the available data for the basin interior, is northern with 2 cms⁻¹ speed (Fig. 5). In the intermediate and bottom layer, the mean vector is northeastern, with a slightly higher speed than in the surface layer (2.7 and 2.6 cms⁻¹) (Fig. 5). The current speed in the small Vranjic basin is lower than in the Bay interior. According to the measurements from 1975 and 1976 (ZORE-ARMANDA *et al.*, 1976), the current magnitudes there are one third of the magnitudes recorded in the Bay interior. A comparison of Fig. 5 and Fig. 3 indicates a dominance of the *sirocco*-induced currents along the vertical.

During strong wind episodes with wind speeds over 5 ms⁻¹ the mean current magnitude

Table 5. Correlation coefficients between wind stress (τ_u, τ_v) and current components (u, v) for the periods with wind speeds over 5 ms⁻¹ during field experiments from 1980 until 1990

station	depth (m)	year	τ_u-u	τ_u-v	τ_v-u	τ_v-v	number of data
1	30	1980	-0.611**	0.257**	0.605**	-0.573**	191
2	10	1980	0.086	-0.150**	-0.216**	0.023	325
	30	1980	-0.574**	0.668**	0.546**	-0.844**	321
3	8	1982	0.824**	-0.508**	-0.714**	0.309**	125
	20	1982	0.676**	-0.833**	-0.586**	0.535**	125
	30	1982	-0.863**	0.356**	0.615**	-0.748**	125
	40	1982	-0.827**	0.862**	0.685**	-0.865**	125
4	8	1982	0.684**	-0.637**	-0.751**	0.750**	125
	15	1982	0.712**	-0.680**	-0.586**	0.791**	125
	22	1982	-0.583**	-0.776**	0.900**	0.817**	125
6	20	1984	0.434**	0.107*	-0.694**	-0.152**	602
7	5	1989	0.329**	-0.197**	-0.361**	0.087*	503
	30	1989	0.330**	-0.125*	-0.036	-0.123*	225
8	5	1988	0.289**	0.485**	-0.251**	-0.313**	237
	20	1988	0.319**	-0.491**	-0.212**	0.572**	237
	30	1988	-0.545**	0.174**	0.597**	-0.021	237
	5	1988	0.272**	-0.387**	-0.017	0.678**	369
	30	1988	0.338**	0.353**	-0.269**	-0.377**	369
	5	1989	0.282**	-0.458**	-0.194**	0.626**	590
	30	1989	0.335**	0.311**	-0.204**	-0.280**	327
	5	1990	-0.083*	-0.079*	0.405**	0.336**	796
	20	1990	-0.104**	0.311**	0.364**	-0.425**	860
	30	1990	-0.227**	0.419**	0.228**	-0.454**	860
9	5	1989	-0.031	0.100	-0.020	-0.069	654
	30	1989	-0.334**	-0.596**	0.412**	0.541**	611

** *significant at level of 99.9%*
* *significant at level 99.5%*
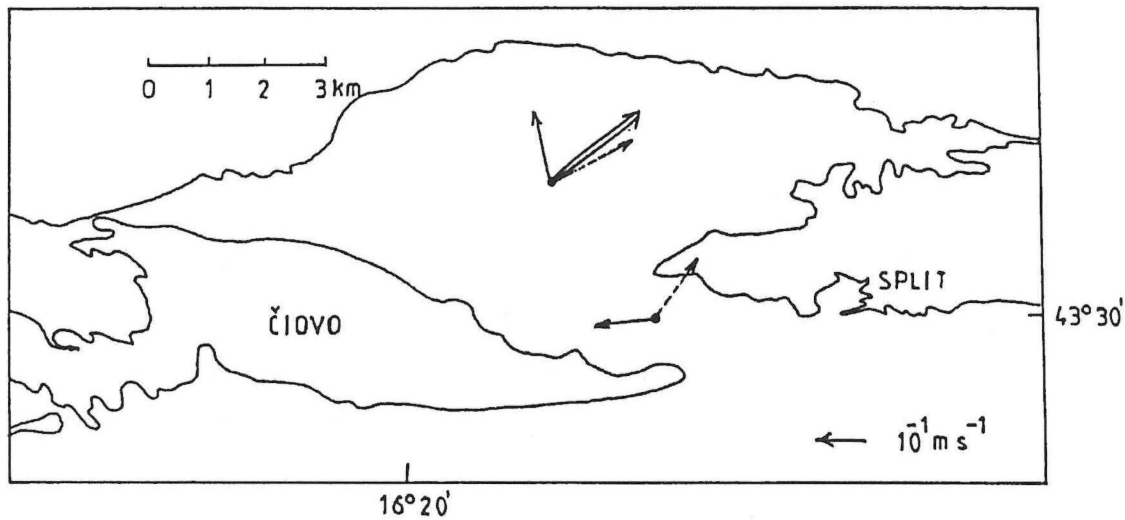
Fig. 5. Mean vectors at the Kaštela Bay inlet and in the Bay interior at the surface layer (full line), the inter-mediate layer (double line) and the bottom layer (dashed line), for the period 1980-1990. Currents in the intermediate layer in the Bay inlet are almost equal to zero

in the Bay inlet is almost twice that of the Bay interior (Figs. 3 and 4). The relation between the currents in the Bay inlet and those in the interior shows the importance of the wind-induced transports from the adjacent Brač channel. Water flowing from the Brač channel toward the Kaštela Bay passes through a relatively narrow inlet and accelerates, due to the conservation of mass.

The analysis of the current data at station 8 (which has the longest time-series) has shown that during the wind episodes with speeds exceeding 5 ms^{-1}, the magnitudes of the current vector in the surface layer are stronger in summer than in winter. This is a consequence of a weaker vertical momentum transfer at the thermocline level (BEG, 1992) (Table 6).

Table 6. Surface currents at the station 8 during periods with wind speeds exceeding 5 ms^{-1}

Dates	u[cms^{-1}]	v[cms^{-1}]	$\sqrt{u^2+v^2}$ [cms^{-1}]	number of data
1988(1) 28 April-7 July	0.65 ± 2.33	3.7 ± 4.10	3.75	237
1988(2) 11 August-20 October	-2.43 ± 4.67	1.9 ± 7.06	3.08	369
1989 3 March-12 May	-0.92 ± 2.74	2.52 ± 4.84	2.68	590
1990 16 Ocotber-19 December	-0.51 ± 3.34	1.80 ± 3.94	1.87	796

In summer, when the water column is stratified, the RICHARDSON number reaches a critical value at the thermocline level, resulting in stronger surface currents than during the homogeneous winter situation when the momentum from the atmosphere is distributed evenly along the water column.

According to the surface salinity distribution, an anticyclonic circulation occurs in the Bay interior during *sirocco*, while a cyclonic circulation prevails during *bora* episodes (ZORE-ARMANDA, 1980). Direct current measurements during *sirocco* events with speeds over 5 ms^{-1} indicate a formation of an anticyclonic gyre (Fig. 3). The existence of a cyclonic gyre cannot be confirmed during *bora* events (Fig. 4).

Analyses of the currents during *sirocco* wind with speed above 5 ms^{-1} indicate that the currents in the Bay interior are deflected to the right of the wind showing the importance of the CORIOLIS force (Fig. 3). A similar current deflection to the right of the wind during *bora* events is weaker, with a considerable variability in the direction (Fig. 4). Differences between magnitudes of the *bora*-induced and *sirocco*-induced currents could arise from the different characteristics of these two wind systems. *Sirocco* blows homogeneously along the whole Adriatic, and the assumption of its homogeneity above Kaštela Bay is quite acceptable. Moreover, *sirocco* has a long fetch and induces strong transport, which affects the current field in the Kaštela Bay, especially in its inlet. In contrast, *bora* blowing from the coast, has a strong orographically-induced spatial variability, which can be observed even in a small area as the Kaštela Bay (JURČEC *et al*, 1986). Therefore, *bora* induces a complex current field in the Kaštela Bay, and only carefully planned set of measurements can resolve this spatial uncertainty.

In order to explain the characteristics of the Kaštela Bay current field on a synoptic time-scale in terms of the linear dynamics in BEG PAKLAR and GAČIĆ (1997) paper, two simple dynamical balances were tested, the EKMAN and viscous balance. The EKMAN balance test was positive in the eastern direction at the station 8 (Table 7). Obtained result shows that simple EKMAN balance is valid occasionally even in a small basin like Kaštela Bay, although the original EKMAN model was designed for deep unbounded basins. Significant positive correlations between the wind stress and bottom currents obtained at some stations point to the possibility of viscouse balance in the water column. The regression analysis gave acceptable values for the bottom friction coefficient $(1.71 \times 10^{-3}$ ms^{-1} and 1.98×10^{-3} ms$^{-1})$ for two stations in the Bay interior with assumption of the viscous balance and linear parameterization of the bottom friction (Table 8). Analyses of the simple dynamical balances did not result in generally acceptable result, which means that current field is under the influence of processes on a different time scales.

Table 7. *Testing of the EKMAN balance, where f is CORIOLS parameter, U and V are vertically averaged currents and H is depth*

	station 4 (E direction)	station 8 (N direction)	station 8 (E direction)
fU [ms^{-2}]	—	0.99×10^{-6}	—
$-fV$ [ms^{-2}]	-2.85×10^{-6}	—	-1.92×10^{-6}
$\tau_x/\rho H$ [ms^{-2}]	-1.86×10^{-6}	—	-1.52×10^{-6}
$\tau_y/\rho H$ [ms^{-2}]	—	0.13×10^{-6}	—

Table 8. Results of the regression analysis for the periods with wind speeds exceeding 5 ms⁻¹. where τ_{ub}, is bottom stress component and r is density

station 4				
linear parametrisation of bottom friction ($\tau_{ub} = \rho r u, u = a\tau_u + b, a = \frac{1}{\rho r}$)				
	a [kg⁻¹m²s]	b [ms⁻¹]	r [ms⁻¹]	coef. corr. between currents and winds
22 m N direction	0.49	-1.61×10^{-3}	1.98×10^{-3}	0.817**
quadratic parametrisation of bottom friction ($\tau_{ub} = \rho C_D u|u|, u|u| = c\tau_u + d, c = \frac{1}{\rho C_D}$)				
	c [kg⁻¹ m³]	d [m²s⁻²]	C_D	coef. corr. between currents² and winds
22 m N direction	0.014	0.10×10^{-4}	70.56×10^{-3}	0.619**
station 8 (1988²)				
linear parametrisation of bottom friction				
	a [kg⁻¹m²s]	b [ms⁻¹]	r [ms⁻¹]	coef. corr. between currents and winds
30 m E direction	0.572	45.17×10^{-3}	1.71×10^{-3}	0.338**
quadratic parametrisation of bottom friction				
	c [kg⁻¹ m³]	d [m²s⁻²]	C_D	coef. corr. between currents² and winds
30 m E direction	0.028	25.21×10^{-3}	35.41×10^{-3}	0.212**
station 8 (1989)				
linear parametrisation of bottom friction				
	a [kg⁻¹m²s]	b [ms⁻¹]	r [ms⁻¹]	coef. corr. between currents and winds
30 m E direction	0.154	28.14×10^{-3}	6.49×10^{-3}	0.335**
quadratic parametrisation of bottom friction				
	c [kg⁻¹ m³]	d [m²s⁻²]	C_D	coef. corr. between currents² and winds
30 m E direction	0.01	14.47×10^{-4}	92.73×10^{-3}	0.375**

** *significant at level of 99.9%*

RESULTS OF THE NUMERICAL EXPERIMENTS

The empirical results emphasise the great importance of the wind-induced currents in the Kaštela Bay. This section presents modelling results of the sea currents induced by *sirocco* and *bora*, the two most frequent and strongest wind systems in the studied area (PENZAR, 1977) and their comparison to the empirical data.
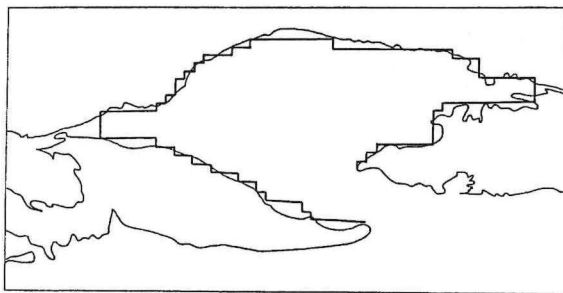
Fig. 6. Domain of the numerical model

The Princeton Ocean Model (POM) (BLUMBERG and MELLOR, 1987) was used for numerical simulation of the wind-induced currents in the Kaštela Bay. Detailed description of the model is given in the ANNEX. In the numerical experiments the barotropic time step was 4 s, whereas the baroclinic time step was 80 s, and both of them satisfied the COURANT-FRIEDRICHS-LEWY computational stability

Table 9. Mean anual temperature distribution (T_A) and summer stratification (T_S and S_S) used in the numerical experiments

H [m]	T_A[^{0}C]	T_S [^{0}C]	S_S [psu]
0.01	17.16	23.00	36.67
5	16.75	21.72	37.00
8	16.54	20.95	37.20
10	16.23	20.44	37.33
15	15.88	18.92	37.54
20	15.54	17.40	37.75
25	15.29	16.70	37.88
30	15.05	16.00	38.00
40	14.81	15.00	38.15
50	14.81	15.00	38.15

condition. The spatial step was chosen to be 300 m, and the whole Bay was covered by a 53x24 point grid (Fig. 6). Twelve sigma layers were assumed in the vertical direction.

Numerical experiments, for both *sirocco* and *bora* forcings, were first performed under assumptions of horizontal and vertical homogeneity of the density field, and the values of the temperature and salinity corresponding to the typical winter values (T=12^{0}C, S=37 psu). Next, the experiments were performed under

Table 10. List of the numerical experiments

experiment	bottom topography	vertical density distribution	wind direction
JHR	flat	homogeneous	SE
JHV	real	homogeneous	SE
JSR	flat	stratification	SE
JSV	real	stratification	SE
BHR	flat	homogeneous	NE
BHV	real	homogeneous	NE
BSR	flat	stratification	NE
BSV	real	stratification	NE

the assumption of a horizontal homogeneous density field and the summer stratification in the vertical direction corresponding to the central Bay station (Table 9). In order to investigate the effect of topography, all the experiments were performed in a flat-bottom basin with 23 m depth, which is the Bay mean depth, and also in the basin with realistic topography. Table 10 lists the experiments.

Sirocco

In the experiment with a flat-bottom basin (JHR) *sirocco* induces spatially homogeneous surface currents in the wind direction, whereas bottom currents are oppositely directed (Fig. 7 a, b). Vertically averaged currents are almost equal to zero (Fig. 7 c). After introducing a realistic topography (experiment JHV) gyres are formed in the surface and in the bottom layer: a cyclonic gyre in the northern part of the basin

and an anticyclonic gyre in the southern part (Fig. 8 a, b). This roughly agrees with numerical results from ORLIĆ *et al.* (1989) and BONE *et al.* (1992). Stronger surface currents occur in shallow coastal areas. Since the wind is assumed to be spatially homogeneous, the gyres are the result of the interaction of the complex basin topography and the wind-induced currents.

When *sirocco* blows above a flat-bottom basin with a typical summer vertical stratification (JSR), the currents in the surface layer are deflected to the right of the wind direction, with unequally distributed compensatory bottom currents (Fig. 9 a, b). In the vertically averaged current field, the cyclonic gyres occur in the western and northern part of the basin, whereas the anticyclonic gyres occur in the eastern and southern basin part (Fig. 9 c). Surface currents in the basin with a realistic topography (JSV)
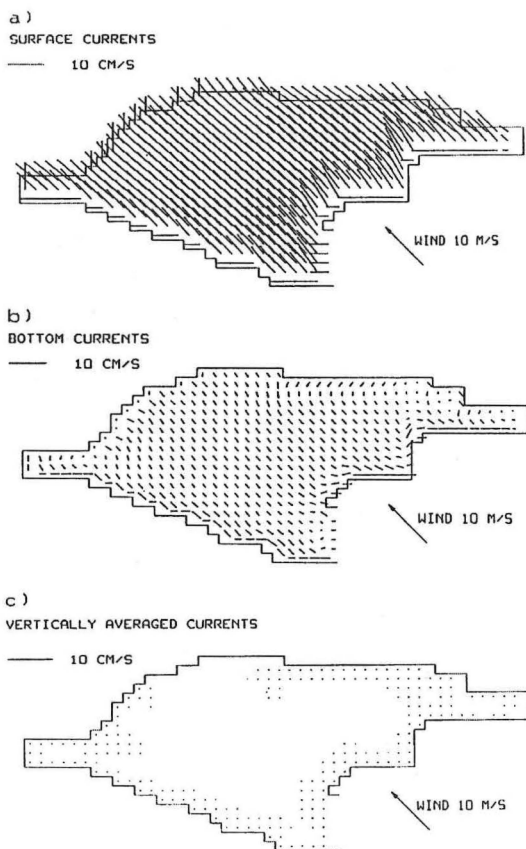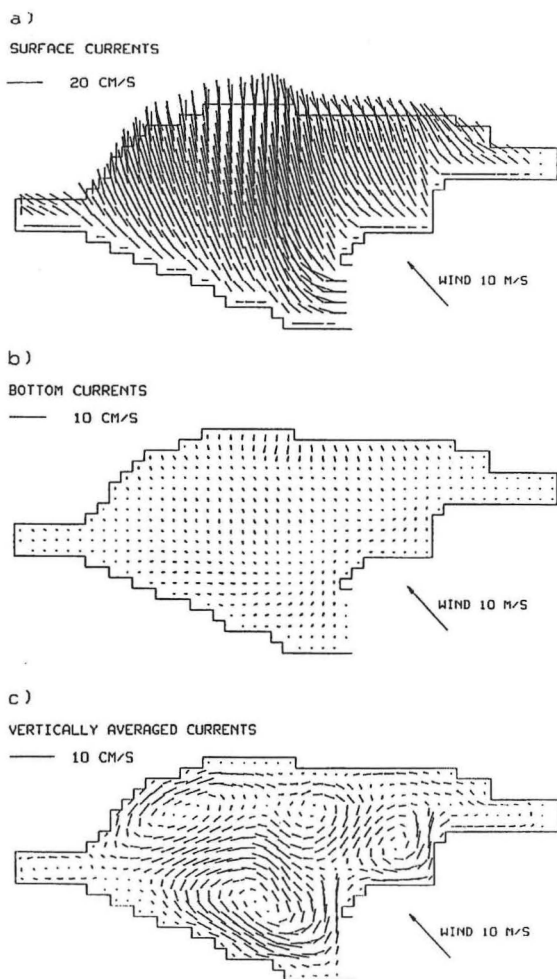

Fig. 7. Surface (a), bottom (b) and vertically averaged currents (c) obtained under the following conditions: sirocco, flat-bottom basin and homogeneous fluid (JHR)
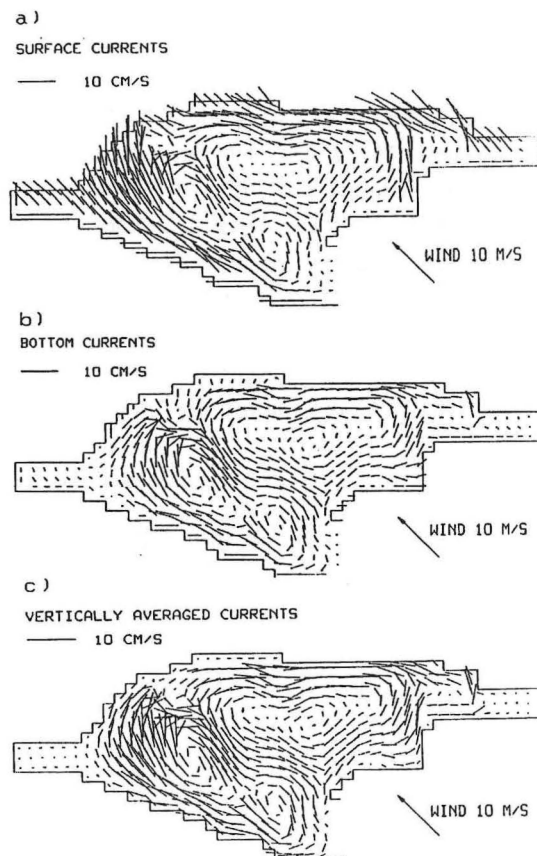
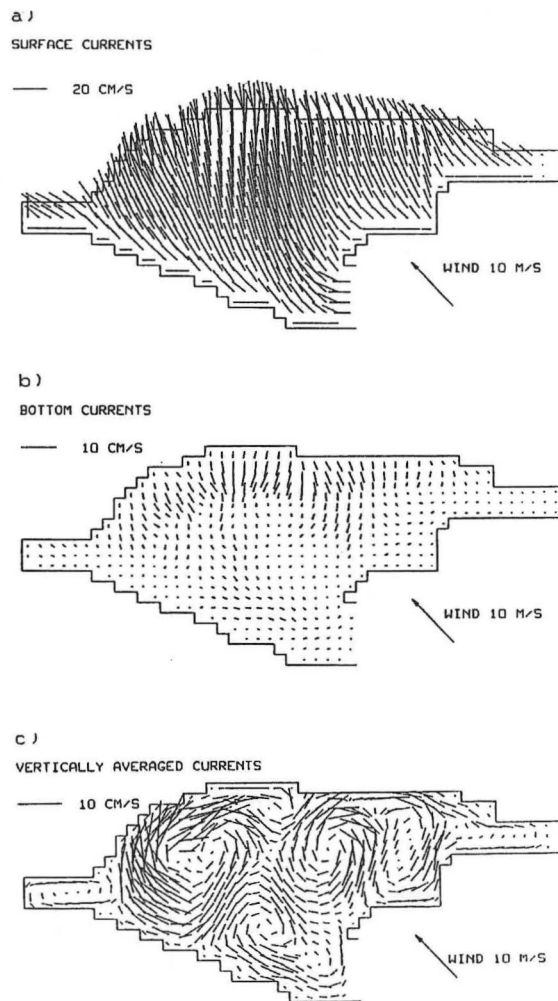*Fig. 8. Surface (a), bottom (b) and vertically averaged currents (c) obtained under the following condition: sirocco, realistic-topography basin and homogeneous fluid (JHV)*

are similar to those simulated in the flat-bottom basin (Fig. 10 a), but with stronger intensities. Current directions in the bottom layer are similar to those in the flat-bottom basin but with stronger intensities in the shallow area (Fig. 10 b). A small cyclonic gyre occurs in the eastern part of the basin. Gyres in the vertically averaged current field have the same shape as those in the flat-bottom basin, but with higher current speeds (Fig. 10 c). The difference between a flat and a variable bottom cases occurs in the eastern part of the basin, where a cyclonic gyre appears when a realistic topography is introduced.

Vertical exchange coefficients of the momentum for the homogeneous and stratificated water column are depicted in Fig. 11. Two experiments were performed for the stratified case: the first one assuming mean annual vertical distribution of temperature and homogeneos salinity and the second one assuming typical summer stratification along the vertical with pronounced thermocline (Table 9). Vertical coefficients obtained in the experiment with the homogeneous density are much higher than those in the stratified sea. In the stratified sea maximal coefficients are in the surface layer up to the thermocline, and have lower values in the

Fig. 9. Surface (a), bottom (b) and vertically averaged currents (c) obtained under the following conditions: sirocco, flat-bottom basin and vertically stratified fluid (JSR)

Fig. 10. Surface (a), bottom (b) and vertically averaged currents (c) obtained under the following conditions: sirocco, realistic-topography basin and vertically stratified fluid (JSV)

a)

b)
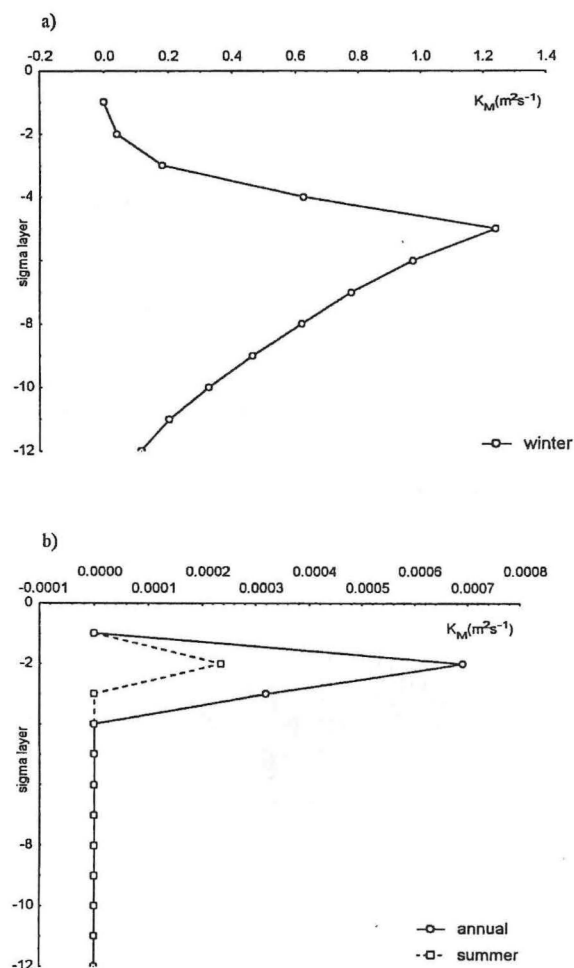
Fig. 11. Vertical distribution of the momentum vertical turbulent exchange coefficients in a homogeneous (a) and stratified (b) sea
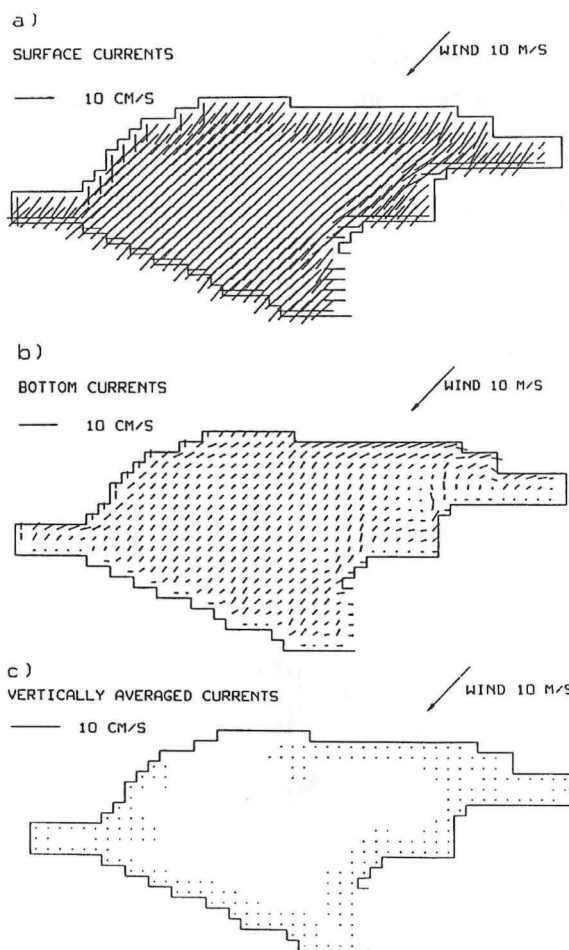
a)

b)

c)

Fig. 12. Surface (a), bottom (b) and vertically averaged currents (c) obtained under the following conditions: bora, flat-bottom basin and homogeneous fluid (BHR)

case of stronger stratification. Turbulent kinetic energy is distributed in the similar way as vertical coefficients. Obtained results are in agreement with empirical results presented in Table 6, showing stronger currents in the surface layer during summer.

Bora

Similar experiments as those for *sirocco* were performed for the *bora* forcing, as well. Result of the BHR experiment are the same as in the case of the *sirocco*-induced currents, with downwind currents in the surface layer and upwind gradient currents in the bottom layer (Fig. 12 a, b). Under *bora* influence in the basin with a realistic topography an anticyclonic gyre appears in the eastern part of the basin, whereas

in the western part a cyclonic gyre forms (Fig. 13 a, b). This is in agreement with the previous numerical model results (ORLIĆ *et al.*, 1989; BONE *et al.*, 1992). It is interesting to notice that at the grid point that corresponds to the position of the station 8, vertically averaged current is in agreement with EKMAN balance, which was obtained from the current measurements (Table 7). Obviously this balance is not valid for most other areas of the Bay.

Under the *bora* influence in a flat-bottom basin with a horizontally homogeneous density field, but with a typical summer vertical stratification (experiment BSR), the currents in the surface layer are deflected to the right of the wind direction, with compensatory currents in
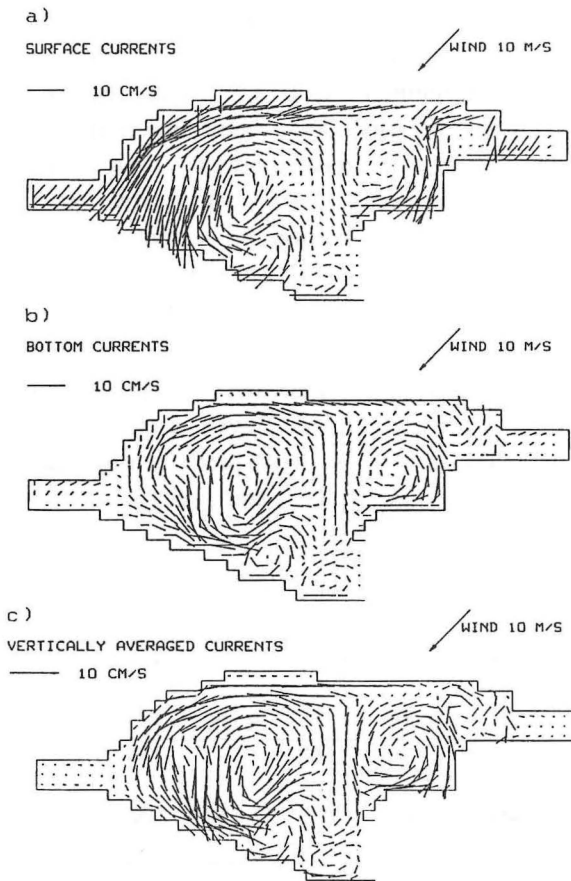
Fig. 13. Surface (a), bottom (b) and vertically averaged currents (c) obtained under the following conditions: bora, realistic-topography basin and homogeneous fluid (BHV)
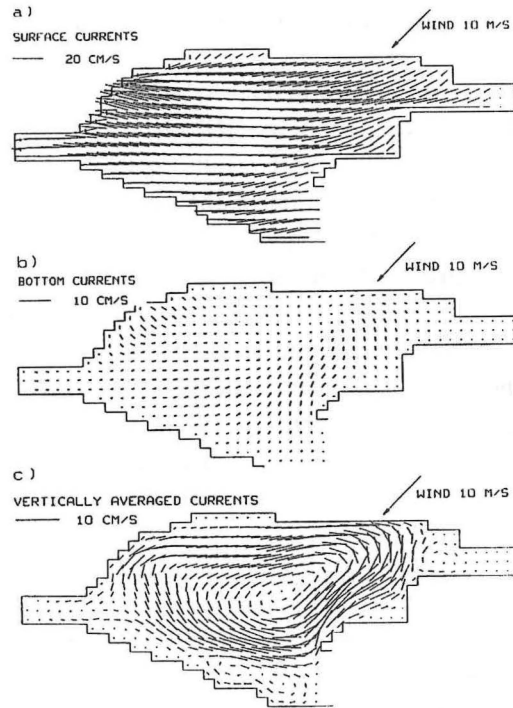

Fig. 14. Surface (a), bottom (b) and vertically averaged currents (c) obtained under the following conditions: bora, flat-bottom basin and vertically stratified fluid (BSR)
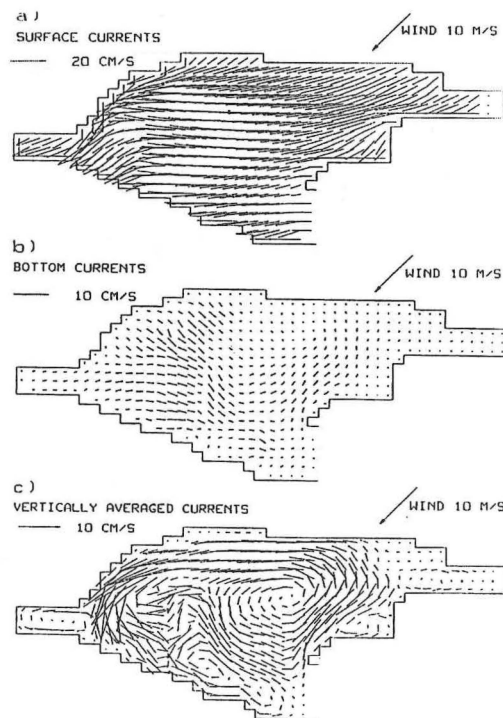

Fig. 15. Surface (a), bottom (b) and vertically averaged currents (c) obtained under the following conditions: bora, realistic-topography basin and vertically stratified fluid (BSV)

the bottom layer (Fig. 14 a, b). A basin-wide cyclonic circulation can be observed in the vertically averaged current field. It results from a complex coastal line and the vertical stratification (Fig. 14 c). In the basin with a realistic topography (experiment BSV), the surface currents under the *bora* influence are similar to those occurring in the flat-bottom case, with the exception in the western part (Fig. 15 a). A small cyclonic gyre is present in the northern part of the basin, in the bottom compensatory layer (Fig. 15 b). A basin-wide cyclonic gyre in the vertically averaged current field is similar to the gyre that appears in the flat-bottom basin, but with a slight difference in the western part of the Bay (Fig. 15 c), where small anticyclonic gyres occur.

Comparison with empirical results

The current flow in the Bay inlet as obtained by the numerical modeling (ORLIĆ *et al.*, 1989; BONE *et al.*, 1992 and results in this paper), depends on the position of the open boundary and on the condition employed on it. Results of all models used for simulation of the wind-induced currents indicate an inflowing current at the surface layer and an outgoing current at the bottom layer, during both *sirocco* and *bora* wind. However the intensity of the flow differs from model to model. Numerically obtained two-layer water exchange with the incoming flow in the surface layer and the outgoing flow in the deeper layer under the *sirocco* influence is in agreement with the measured flow. Although the modelled current directions are in agreement with measurements, their magnitudes are too weak. During *bora* a prevalence of the measured weak outgoing current in the surface layer was not confirmed by either of the numerical models.

The surface salinity analysis (ZORE-ARMANDA, 1980) indicates a formation of a basin-wide anticyclonic gyre during *sirocco* episodes. In contrast, POM predicts a formation of several small cyclonic and anticyclonic gyres

Table 11. Mean current component values ($\overline{E5}$, $\overline{N5}$, $\overline{E20}$, $\overline{E30}$, $\overline{N30}$,) at station 8 with corresponding standard deviations (σ) and root mean squared errors (RMS). All values are given in cms^{-1}

exp.	$\overline{E5}$		$\overline{N5}$		$\overline{E20}$		$\overline{N20}$		$\overline{E30}$		$\overline{N30}$	
	$\pm\sigma$	RMS	$\pm\sigma$	RMS	$\pm\sigma$	RMS	$\pm\sigma$	RMS	$\pm\sigma$	RMS	$\pm\sigma$	RMS
JHV	1.819		2.392		3.519		-0.453		2.662		-1.869	
	1.626	1.717	2.379	5.377	1.309	1.314	1.404	3.364	2.006	2.134	1.825	2.447
JHV1		2.108		3.082		3.506		1.706		3.124		1.878
JSV	-4.972		9.317		4.486		1.298		3.154		-3.690	
	7.051	7.055	5.306	32.943	0.645	17.068	1.420	12.509	3.122	3.833	1.167	1.404
JSV1		7.152		16.229		9.033		3.258		3.883		1.221
JSV2		9.293		5.467		4.289		3.343		4.230		2.288
BHV	-3.103		0.609		0.948		2.430		0.504		0.317	
	4.243	4.256	1.514	1.538	2.440	3.594	2.013	2.107	0.425	2.215	0.525	1.592
BHV1		4.302		1.535		4.818		2.180		3.708		1.391
BHV2		4.421		2.479		5.252		3.228		4.198		0.655
BHV3		4.306		1.705		2.480		3.218		0.492		0.525
BSV	-3.506		-5.207						3.811		0.462	
	2.978	39.507	2.041	8.127					3.878	3.700	3.644	4.805
BSV1		4.221		7.103						5.172		3.726
BSV2		4.098		2.991						4.475		3.748

that result from the interaction of the complex basin coastal line, topography, wind stress and density gradients. The numerical model results in the stratified sea partially agree with the results of the direct current measurements in the surface and bottom layers (Figs. 3 and 10). The formation of several small gyres of both orientations was not observed during currentmeter measurements, only an indication of a basin-wide anticyclonic gyre.

Beside qualitative comparison similar to one performed by ORLIĆ *et al.* (1998), quantitative comparison between modelled and measured currents was also made. Since current data are the most numerous at the northernmost station 8, results obtained there are used for the comparison. First currents during the wind periods with speeds over 7 ms^{-1} were extracted from the complete data set. Extracted data were grouped into the four groups according to the

prevailing wind and vertical density distribution in the Bay: winter *sirocco*, characterized by vertical homogeneous water column, summer *sirocco* with pronounced thermocline and winter and summer *bora*. To achieve better agreement between modelled and measured currents, new numerical experiments with different stratifications, wind stresses, and vertical energy distribution were performed. Discrepancy between modelled and realistic data is presented in terms of root mean squared (RMS) error (Table 11).

Currents obtained during winter *sirocco* episodes are shown on the left side of Fig. 16. The agreement between these currents and those obtained under the same conditions by the numerical model (JHV experiment) is low in the surface layer, whereas in the bottom layer agreement is acceptable. Introducing week stratification in the experiment (JSV1) with
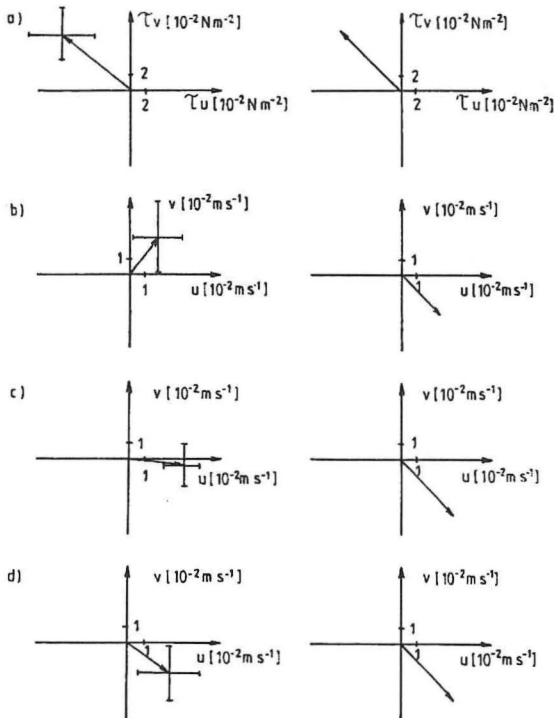

Fig. 16. Mean wind stress during all considered winter sirocco episodes (a, left) and wind stress used in the numerical experiment JHR (a, right). Comparison of the mean measured (left) and modelled (right) currents at 5 m (b), 20 m (c) and 30 m (d). Horizontal and vertical lines at the vector end denote standard deviations of the measured values
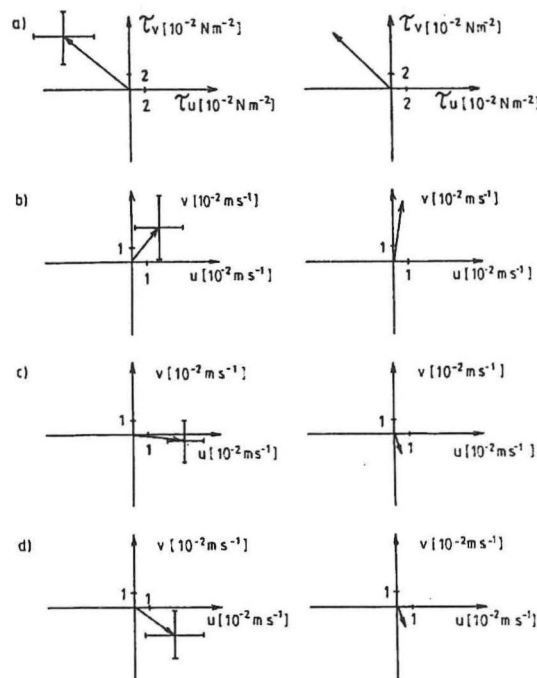
Fig. 17. Mean wind stress during all considered winter sirocco episodes (a, left) and wind stress used in the numerical experiment JHR1 (a, right). Comparison of the mean measured (left) and modelled (right) currents at 5 m (b), 20 m (c) and 30 m (d). Horizontal and vertical lines at the vector end denote standard deviations of the measured values

temperature according mean annual distribution (Table 9) and homogeneous salinity, modelled surface current fall into the standard deviation interval around mean measured value (Fig. 17). Better agreement between surface current obtained in JSV1 experiment and the measured one is reflected in decrease of RMS error in the northern direction (Table 11).

Agreement between measured and modelled currents during summer *sirocco* episodes (Fig. 18) is the best of all considered situations in the surface and bottom layer. Three experiments were performed for the case of *sirocco* blowing above stratified sea: JSV experiment whose results are shown on the Fig. 10, JSV1 experiment with wind stress according to the mean wind stress during all *sirocco* episodes in summer, and JSV2 experiment with 50% lower drag coefficient than in JSV1 experiment. High RMS errors were obtained in surface and inter-

mediate layer in JSV and JSV1 experiments, whereas significant RMS decrease is obtained lowering drag coefficient. Lower drag coefficient could result from the fact that during summer atmosphere above the sea is stable, which results in the lower momentum exchange at the atmosphere - sea interface.

The formation of a *bora*-induced, basin-wide cyclonic gyre, as derived from the numerical model in the stratified sea, agrees with ZORE-ARMANDA (1980) salinity analyses. However, the more recent current measurements with AANDERAA currentmeters did not confirm the previous results. These measurements indicate the presence of low speed currents with a strong horizontal variability (Fig. 4).

Agreement between modelled and measured currents at the station 8 during winter *bora* episodes is good in the surface layer, whereas in the bottom layer measured current is
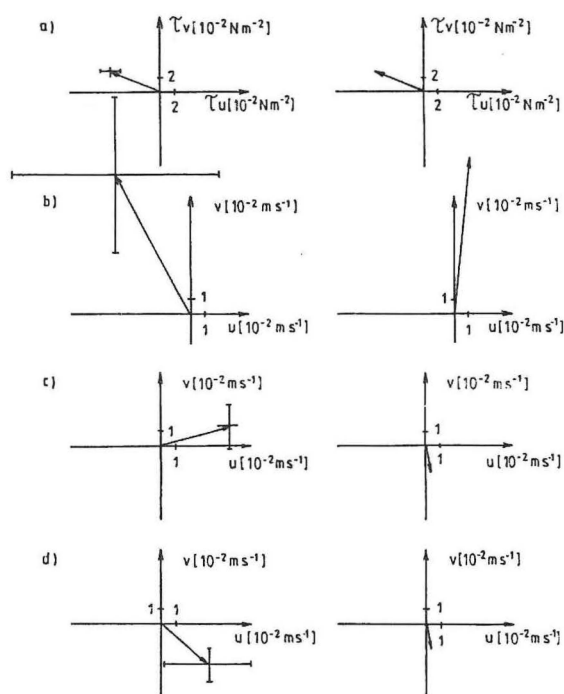

Fig. 18. Mean wind stress during all considered summer sirocco episodes (a, left) and wind stress used in the numerical experiment JSR2 (a, right). Comparison of the mean measured (left) and modelled (right) currents at 5 m (b), 20 m (c) and 30 m (d). Horizontal and vertical lines at the vector end denote standard deviations of the measured values
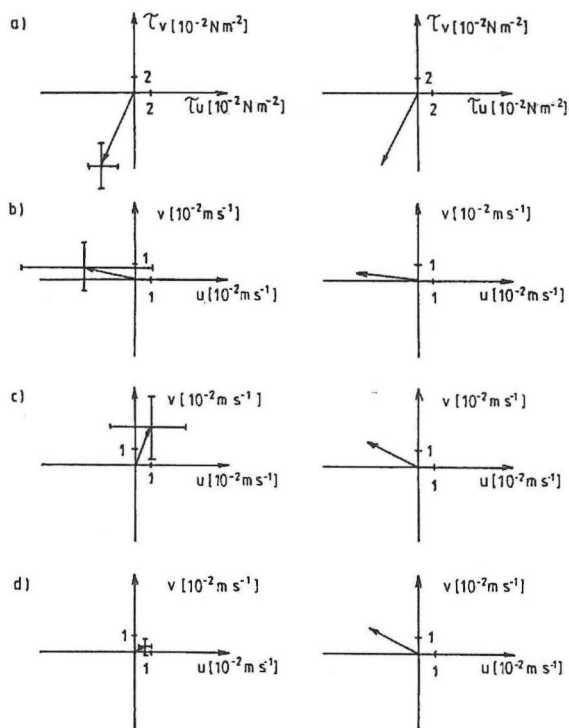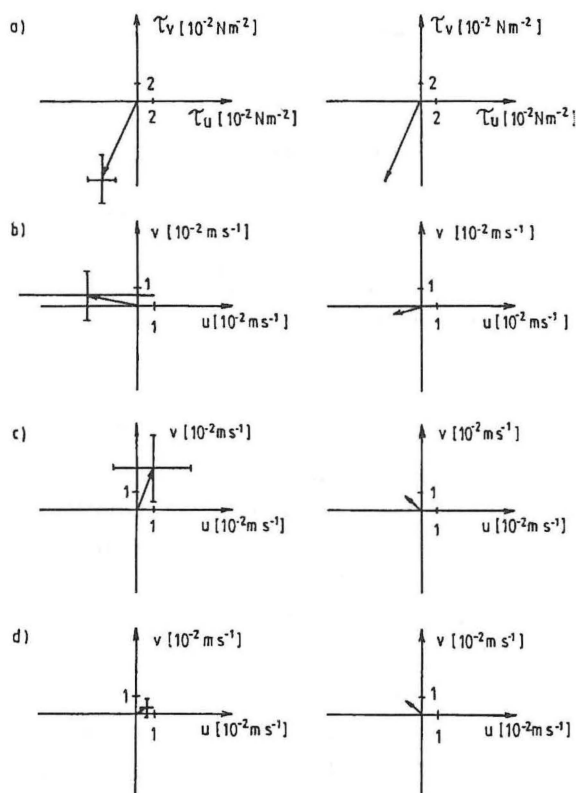
Fig. 19. Mean wind stress during all considered winter bora episodes (a, left) and wind stress used in the numerical experiment BHR (a, right). Comparison of the mean measured (left) and modelled (right) currents at 5 m (b), 20 m (c) and 30 m (d). Horizontal and vertical lines at the vector end denote standard deviations of the measured values

much lower than the modelled with about 90^0 difference in the direction (experiment BHV, Fig. 19). Increasing bottom friction leads to the lowering of bottom and also of the surface current (experiment BHV1, Fig 20). Obtained lower surface value still falls into the interval of standard deviation around the mean measured value. Strong decrease of the bottom turbulent coefficients for four orders of magnitude gave modelled value comparable to the measured one in the bottom layer (experiment BH2, Fig. 21). RMS errors in the surface and intermediate layers for BHV and BHV1 experiments are of the order of magnitude of the standard deviation, whereas RMS errors in the bottom layer are much higher than corresponding standard deviations (Table 11). With increasing bottom fric-
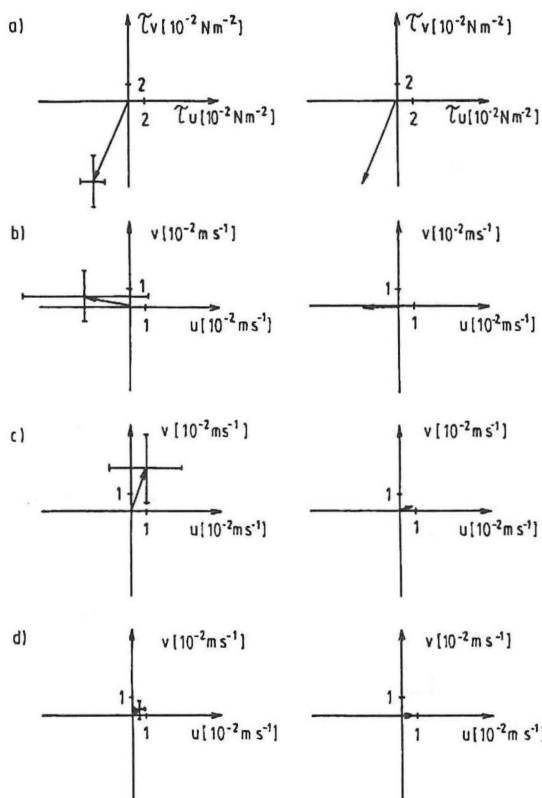

Fig. 21. Mean wind stress during all considered winter bora episodes (a, left) and wind stress used in the numerical experiment BHR2 (a, right). Comparison of the mean measured (left) and modelled (right) currents at 5 m (b), 20 m (c) and 30 m (d). Horizontal and vertical lines at the vector end denote standard deviations of the measured values

tion in experiment BHV1, RMS errors in the surface and intermediate layer increase, whereas in the bottom layer RMS decrease. The best agreement of the model results with measured currents, with lowest RMS errors, is obtained by strong decrease of the turbulent exchange coefficients in the bottom layer.

Modelled surface current during summer *bora* episodes is rotated to the right of the measured current for about 90^0. Modelled bottom current is also rotated to the right of the measured one and it is of much lower intensity. This discrepancy between modelled and measured values result in high RMS errors for BSV experiment, whose results are shown on Fig. 14. In the experiment with lower values of drag coefficients RMS errors decrease (BSV1 experiment, Fig. 22), but the modelled current directions
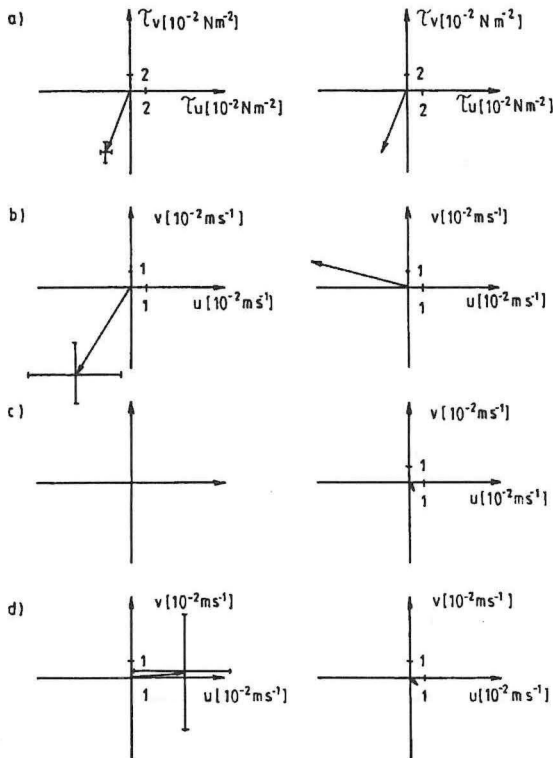

Fig. 20. Mean wind stress during all considered winter bora episodes (a, left) and wind stress used in the numerical experiment BHR1 (a, right). Comparison of the mean measured (left) and modelled (right) currents at 5 m (b), 20 m (c) and 30 m (d). Horizontal and vertical lines at the vector end denote standard deviations of the measured values
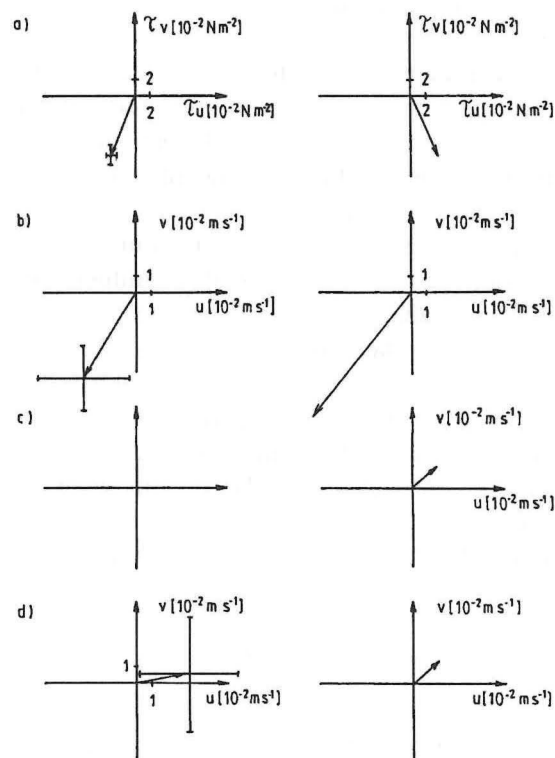
Fig. 22. Mean wind stress during all considered summer bora episodes (a, left) and wind stress used in the numerical experiment BSR1 (a, right). Comparison of the mean measured (left) and modelled (right) currents at 5 m (b), 20 m (c) and 30 m (d). Horizontal and vertical lines at the vector end denote standard deviations of the measured values

Fig. 23. Mean wind stress during all considered summer bora episodes (a, left) and wind stress used in the numerical experiment BSR2 (a, right). Comparison of the mean measured (left) and modelled (right) currents at 5 m (b), 20 m (c) and 30 m (d). Horizontal and vertical lines at the vector end denote standard deviations of the measured values

still differ from the empirical data. The best agreement with measured currents, with lowest RMS, is obtained in the experiment with wind blowing from north-northwest direction (BSV2 experiment, Fig. 23). These results open the question whether the wind data from the meteorological station Marjan are applicable for the whole Kaštela Bay.

DISCUSSION AND CONCLUSIONS

Since mean current vectors obtained from all available current data coincide with *sirocco*-induced currents, the importance of the *sirocco* for the formation of the Kaštela Bay current field is obvious. The reason for a strong *sirocco* influence on the currents is Bay geometry and location with inlet exposed to *sirocco* influence. Two layer circulation during *sirocco* events in

the Bay inlet, with the incoming flow at the surface layer, and the outgoing flow in the deeper layers, results from the turbulent vertical exchange of momentum and the pressure gradient force. It is confirmed both by hydrographic analyses (ZORE-ARMANDA, 1980) and direct current measurements (GAČIĆ, 1982; GAČIĆ *et al.*, 1987; BEG PAKLAR and GAČIĆ, 1997). In that way *sirocco* reverses typical estuarine circulation. A superposition of the two oppositely directed current systems: the gravitational and the wind-induced, results in a considerable horizontal variability of the currents in the inlet. Direct current measurements indicate that a horizontal current compensation in the Bay inlet occurs during periods with stratified water column, whereas a two layer circulation dominants during periods of homogeneous water col-

umn. *Sirocco* substantially increases the speed of the water exchange between the Kaštela Bay and the adjacent Brač channel.

On the other hand, *bora* influence on the Bay inlet is difficult to define due to orientation of the Bay inlet and complex orography around it. A prevalence of a weak outgoing flow in the surface layer is confirmed both by the hydrographic (ZORE-ARMANDA, 1980) and the current data analysis (BEG PAKLAR and GAČIĆ, 1997).

Complex topography generates vorticity in the wind-induced current field inside the Bay. The vorticity is confirmed by the surface salinity analysis (ZORE-ARMANDA, 1980), which showed a cyclonic circulation during *bora* events and an anticyclonic circulation during *sirocco*. The currentmeter data from the 1980's show some agreement with previous results during *sirocco* events, whereas this agreement is poor during *bora* events. The currentmeter measurements showed a deflection of the surface current vector to the right of the wind direction during *sirocco*, pointing to the importance of the CORIOLIS force, whereas during *bora* small variable currents were recorded.

The vorticity in the wind-induced current field is also confirmed by the modelling results. Gyres are present in almost all numerical experiments performed in this paper. In a homogeneous fluid, the gyres result from the interaction of topography and wind-induced currents, and are not present in the flat-bottom basin. The complex current fields induced by both *sirocco* and *bora* in the homogeneous fluid can be explained in terms of a simple analytic model for bottom-slope currents (WEENINK, 1958; WEENINK and GROEN, 1958; ORLIĆ *et al.*, 1989). In the shallow parts, transports are in the downwind direction, whereas in the deeper parts, transports are upwinded. The Kaštela Bay coastal line and basin topography are so complex that a change in the wind direction leads to considerable changes in the current field, as can be seen by comparing the modelled *sirocco*- and *bora*- induced currents. Two experiments were performed with coarser grid resolution of 600 m assuming that *bora* and *sirocco* blow above horizontally and vertically homogeneous
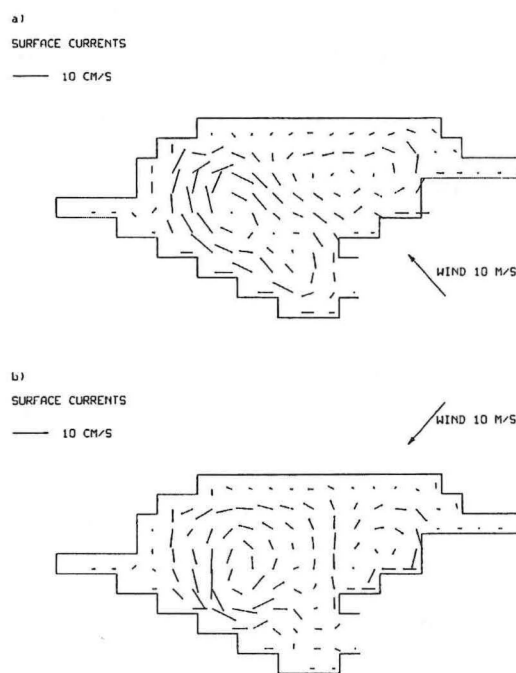

Fig. 24. Surface currents obtained in the realistic-topography basin during winter sirocco (a) and winter bora (b) on the 600 m resolution grid

sea (Fig. 24). Obtained gyres are almost the same as those in the experiments with 300 m resolution, showing that the structures really result from the complex topography and coastline. In a stratified fluid, gyres result from the density gradients, topography and wind stress, and are present even in the flat-bottom basin. The influence of topography on the wind-induced currents is more pronounced in the vertically homogeneous fluid. Basin-wide cyclonic circulation obtained in the experiment with *bora* blowing above vertically stratified sea is in agreement with the conclusion of the salinity measurement analysis. Several cyclonic and anticyclonic gyres were generated in the experiment with *sirocco* wind, which is partly in agreement with anticyclonic gyre predicted from salinity distribution.

Modelling results can only partially be compared with the currentmeter measurements. Although measurements with AANDERAA currentmeters have brought new and valuable knowledge of the Kaštela Bay current field, and

especially stressed the importance of the wind-induced currents, their low horizontal resolution makes it difficult to compare their results to the surface salinity analyses and the results of the numerical experiments. The other disadvantage of the direct current measurements arises from the fact that the currents were measured at different stations and in different seasons, which prompts question regarding their comparability. This should be taken into account in planning future field experiments.

The currentmeter data obtained at the northernmost station 8 are the most numerous and therefore are compared with numerical model results. Comparison between modelled and measured data indicates that proper prediction of the wind-induced currents demands detailed knowledge of the wind stress above Kaštela Bay and of the density distribution in the sea. Lower drag coefficient values in summer than in winter, due to the stable atmosphere above the sea in summer, for both *sirocco* and *bora* wind, result in much better agreement between modelled and measured data. During winter *sirocco* episodes weak stratification in the numerical experiments gave good results, whereas during winter *bora* strong energy decrease in the bottom layer increase agreement between modelled and measured currents.

The difference between wind-induced currents that result from three numerical models (ORLIĆ *et al.*, 1989; BONE *et al.*, 1992 and results presented here) indicate that physical and numerical background must be carefully designed, together with model parameterisation. Gyres obtained in a homogeneous fluid in the vertically averaged current fields are almost the same in all three models. The intensity of the gyres varies, depending on the particular model used and on the assumed vertical stratification. The differences arise in homogeneous sea in the surface layer, where the HEAPS model predicts spatially homogeneous currents deflected to the right of the wind direction, whereas the other two models predict topographically induced gyres. Surface currents obtained with the HEAPS model agree with POM-predicted currents in a stratified fluid.

Future numerical experiments should take into account better formulation of the open boundary conditions, obtained from the direct current measurements or from the sea level data, together with surface heat and water fluxes, pronounced during realistic *bora* episodes. The proper numerical model verification in more than one point and also a better understanding of the dynamics of the wind-induced currents demand careful planning of the field experiments. The results of the direct current measurements also confirm the importance of the pressure gradient force (BEG, 1992). Future measurements should provide data for its estimation.

ACKNOWLEDGEMENTS

REFERENCES

BEG, G. 1992. Utjecaj vjetra i tlaka zraka na strujno polje Kaštelanskog zaljeva. Magistarski rad, Sveučilište u Zagrebu, 149 pp.

BEG PAKLAR, G. and M. GAČIĆ. 1997. The wind effect on the Kaštela Bay current field. Acta Adriat., 38(2): 31-43.

BONE, M. 1993. Development of a non-linear levels model and its application to *bora*-driven circulation on the Adriatic shelf. Estuar. Coast. Shelf Sci., 37: 475-496.

BONE, M., G. BEG, A. SMIRČIĆ and M. UVODIĆ. 1992. Modelska studija struja drifta za područja Bračkog i Splitskog kanala i Kaštelanskog zaljeva. Studije i elaborati (Technical report), 122. Institut za oceanografiju i ribarstvo, Split, 209 pp.

BERGAMACSO, A. and M. GAČIĆ. 1996. Baroclinic response of the Adriatic Sea to an episode of *bora* wind. J. Phys. Ocean., 26: 1354-1369.

BLUMBERG, A. and G.L. MELLOR. 1983. Diagnostic and prognostic numerical circulation studies of the South Atlantic Bight. J. Geophys. Res., 88(C8): 4579-4592.

BLUMBERG, A. and G.L. MELLOR. 1987. A description of a three-dimensional coastal ocean circulation model. In: Heaps N.S, (Editor). Three Dimensional Coastal Ocean Models. Coastal and Estuarine Science, 4, American Geophysical Union, Washington, D.C. pp.16.

DEACON, E.L. and E.K. WEBB. 1962. Interchange of properties between sea and air. The Sea, Vol 1, Hill M.N. (Editor). Interscience Publisher, 43-315.

GAČIĆ, M. 1982. Notes on characteristics of the response of near-shore current field to the onshore wind. Bilješke - Notes, Institute of Oceanography and Fisheries, Split, 47: 6 pp.

GAČIĆ, M. and A. SMIRČIĆ. 1973. Statistička analiza dinamike površinskog sloja Kaštelanskog zaljeva. Hidrogr. godišn., 71: 89-102.

GAČIĆ, M., V. DADIĆ, N. KRSTULOVIĆ, I. MARASOVIĆ, M. MOROVIĆ, T. PUCHER-PETKOVIĆ and N. SVILIČIĆ. 1987. Near shore transport processes induced by the wind. Estuar. Coast. Shelf Sci., 24: 35-46.

GAČIĆ, M., B. GRBEC and V. DADIĆ. 1991. Wind induced currents in an inlet of a semi-enclosed bay (Kaštela Bay, Adriatic Sea). Acta Adriat. 32(2): 607-620.

JURČEC, V., A. BAJIĆ and K. PANDŽIĆ. 1986. Simulacija bure i juga u srednjem Jadranu. Hidrogr. godišn., 1984-1985: 59-71.

MELLOR, G.L. 1991. An equation of state for numerical models of ocean and estuaries. Journal of Atmospheric and Oceanic Technology, 8: 609-611.

MELLOR G.L. and T. YAMADA. 1982. Development of turbulent closure models for geophysical fluid problems. Reviews of Geophysics and Space Physics, 20(4): 851-875.

MELLOR G.L. and A.F. BLUMBERG. 1985. Modeling vertical and horizontl diffusivities

with the sigma coordinate system. Monthly Weather Review, 113: 1379-1383.

OEY, L.Y., G.L. MELLOR and R.I. HIRES. 1985a. A three-dimensional simulations of the Hadson-Raritan estuary. Part I: Description of the model and model simulations. J. Phys. Ocean.,15: 1676-1692.

OEY, L.Y., G.L. MELLOR and R.I. HIRES. 1985b. A three-dimensional simulations of the Hadson-Raritan estuary. Part II: Comparison with observation. J. Phys. Ocean., 15: 1693-1709.

OEY L.Y., G.L. MELLOR and R.I. HIRES. 1985c. A three-dimensional simulations of the Hadson-Raritan estuary. Part III: Salt flux analyses. J. Phys. Ocean., 15: 1711-1720.

ORLIĆ, M., M. KUZMIĆ and Z. PASARIĆ. 1989. Modelling wind-driven transports in the Kaštela Bay. UNEP Mediterranean action plan, Priority action programme, Regional activity centre Split. CPP/1988-1989/YU/DOC. 3A, 43 pp.

ORLIĆ, M., M. KUZMIĆ and Z. PASARIĆ. 1998. Modeliranje vjetrovnog strujanja u Kaštelanskom zaljevu. Zbornik "Kaštela - kolijevka Hrvatske", 367-372.

PENZAR, B. 1977. Tlak zraka - Vjetar. Prilozi poznavanju vremena i klime SFRJ, 2: 1-117.

PRITCHARD, D.W. 1954. A study of the salt balance of a coastal plain estuary. J. Mar. Res., 13(1): 133-144.

PRITCHARD, D.W. 1956. The dynamic structure of a coastal plain estuary. J. Mar. Res., 15(1): 33-42.

RATTRAY, M. and D.V. HANSEN. 1965. Gravitational circulation in straits and estuaries. J. Mar. Res., 23(2): 104-121.

SIMONS, T.J. 1974. Verification of numerical models of Lake Ontario. Part 1. Circulation in spring and early summer. J. Phys. Ocean., 4: 507-523.

WANG, D.P. 1979. Wind-driven circulation in the Chesapeak bay, Winter 1975. J. Phys. Ocean., 9(3): 564-572.

WEATHERLY G. L. and P. J. MARTIN. 1978. On the structure and dynamics of the oceanic bottom boundary layer. J. Phys. Ocean., 8: 557-570.

WEENINK, M.P.H. 1958. A theory and method of calculation of wind effects on sea levels in a partly-enclosed sea, with special application to the southern coast of the North Sea. Koninklijk Nederlands Meteorologisch Institut - Mededelingen en Verhandelingen, 73: 1-111.

WEENINK, M.P.H. and P. GROEN. 1958. A semitheoretical, semi-empirical approach to the problem of finding wind effects on water levels in a shallow partly-enclosed sea. Proceedings-Koninklijke Academie van Wetenschappen, B61: 198-213.

WINANT, C.D. 1980. Coastal circulation and wind-induced currents. Ann. Rev. Fluid Mech., 12: 271-301.

ZORE-ARMANDA, M. 1980. Some dynamic and hydrographic properties of the Kaštela Bay. Acta Adriat., 21 (2):55-74.

ZORE-ARMANDA, M. 1986. Karakteristike strujanja istočno-jadranskog priobalja. Pomorski zbornik, 24: 387-406.

ZORE-ARMANDA, M., M. BULJAN, S. ALFIREVIĆ, J. KARLOVAC, T. PUCHER-PETKOVIĆ and T. VUČETIĆ, 1969. Kompleksno istraživanje morskih struja u Jadranu. Institut za oceanografiju i ribarstvo, Stručni izvještaj, 88 pp.

ZORE-ARMANDA, M. (Editor). et al. 1974. Oceanografska istraživanja mora kod Splita. Vol. I, Studije i elaborati (Technical report) 6, Institut za oceanografiju i ribarstvo, Split, 119 pp.

ZORE-ARMANDA, M. (Editor). et al. 1976. Oceanografsko-biološka svojstva mora i epidemiološko-bakteriološka svojstva otpadnih voda sjevernog slivnog područja Splita. Vol. I, Studije i elaborati (Technical report) 24, Institut za oceanografiju i ribarstvo, Split, 100 pp.

Struje u Kaštelanskom zaljevu: empirijska analiza i rezultati numeričkog modela

Gordana BEG PAKLAR, Mira ZORE-ARMANDA i Vlado DADIĆ

Institut za oceanografiju i ribarstvo, P. P. 500, 21000 Split, Hrvatska

SAŽETAK

Osnovni statistički podaci o strujama izmjerenim u Kaštelanskom zaljevu u razdoblju od 1953. do 1990. godine ukazuju na veliki značaj juga na strujanje u Kaštelanskom zaljevu. Jugo okreće tipičnu estuarijsku cirkulaciju u vratima zaljeva. Za vrijeme jakih epizoda juga uočena je polarizacija struja u vratima zaljeva u smjeru istok-zapad, sa strujom niz vjetar u površinskom sloju i kompenzacijskom strujom na većim dubinama. U središtu zaljeva površinske struje generirane jugom zakreću nadesno od vjetra pod utjecajem CORIOLIS-ove sile. Srednji iznosi struja u središtu zaljeva za puhanja vjetrova s brzinom većom od 5 ms⁻¹ gotovo su dvostruko manji od onih izmjerenih u vratima zaljeva za puhanja vjetrova iste brzine, što govori o važnosti utjecaja transporta iz okolnog Bračkog kanala.

Numerički dobiven ciklonalni vrtlog na području cijelog bazena za puhanja bure u skladu je sa zaključkom iz analize polja saliniteta. Numerički rezultati pokazuju formiranje nekoliko ciklonalnih i anticiklonalnih vrtloga za puhanja juga, pa se barem u dijelu zaljeva numerički i empirijski rezultati dobiveni iz analize saliniteta podudaraju. Usporedba rezultata mjerenja s rezultatima hidrodinamičkog numeričkog modela daje bolje podudaranje direktno izmjerenih i simuliranih struja za puhanja juga nego za bure. Za ispravnu prognozu vjetrovnih struja potrebno je detaljno poznavati iznos i smjer napetosti vjetra nad Kaštelanskim zaljevom, kao i polja gustoće u bazenu.

Ključne riječi: Kaštelanski zaljev, struje, bura, jugo

ANNEX

POM is a three-dimensional model with the complete nonlinear thermodynamic. The model is based on the momentum equation with BOUSSINESQ and hydrostatic approximation, the continuity equation, the conservation equations for heat and salt coupled with the equation of state (MELLOR, 1991). Vertical turbulent exchange coefficients are provided using the second-order turbulence closure submodel 'Level 2 1/2' (MELLOR and YAMADA, 1982). POM uses a sigma coordinate system with the bottom following vertical coordinate

($\sigma = \dfrac{z-\eta}{z+H}$, where z is the vertical coordinate, H represents the bottom topography, and η is the surface denivelation). The upper coordinate surface is the free sea surface ($\sigma = 0$), whereas the lower coordinate surface is the sea bottom ($\sigma = -1$). The sigma coordinate system is convenient for the simulations in the areas with variable topography, since a high vertical resolution can be achieved even in the shallow areas, without increasing the vertical resolution in the deep regions. A combination of the sigma coordinate system and the turbulence closure model gives good results in modelling the surface and bottom boundary layers, which is very often a source of errors in modelling the wind-induced currents in the coastal regions.

The momentum equation in the sigma coordinate system is as follows (BLUMBERG and MELLOR, 1983, 1987):

$$\frac{\partial uD}{\partial t}+\frac{\partial u^2 D}{\partial x}+\frac{\partial uvD}{\partial y}+\frac{\partial u\omega}{\partial \sigma}-fvD+gD\frac{\partial \eta}{\partial x}=$$

$$=\frac{\partial}{\partial \sigma}\left[\frac{K_M}{D}\frac{\partial u}{\partial \sigma}\right]-\frac{gD^2}{\rho_o}\int_\sigma^0\left[\frac{\partial \rho'}{\partial x}-\frac{\sigma'}{D}\frac{\partial D}{\partial x}\frac{\partial \rho'}{\partial \sigma'}\right]d\sigma'+F_x \quad ,(1)$$

$$\frac{\partial vD}{\partial t}+\frac{\partial uvD}{\partial x}+\frac{\partial v^2 D}{\partial y}+\frac{\partial v\omega}{\partial \sigma}+fuD+gD\frac{\partial \eta}{\partial y}=$$

$$=\frac{\partial}{\partial \sigma}\left[\frac{K_M}{D}\frac{\partial v}{\partial \sigma}\right]-\frac{gD^2}{\rho_o}\int_\sigma^0\left[\frac{\partial \rho'}{\partial y}-\frac{\sigma'}{D}\frac{\partial D}{\partial y}\frac{\partial \rho'}{\partial \sigma'}\right]d\sigma'+F_y \quad ,(2)$$

where u and v are the velocity components in the horizontal plane, $D=H+\eta$ is depth, f is the CORIOLIS parameter, g is the acceleration due to the gravity, ρ is density, K_M is the coefficient of the vertical momentum exchange, F_X and F_Y are the components of the horizontal diffusion, and ω is the velocity component normal to the sigma plane.

$$\frac{\partial Du}{\partial x}+\frac{\partial Dv}{\partial y}+\frac{\partial \omega}{\partial \sigma}+\frac{\partial \eta}{\partial t}=0 \quad , \quad (3)$$

The continuity equation is:

$$\frac{\partial TD}{\partial t}+\frac{\partial TuD}{\partial x}+\frac{\partial TvD}{\partial t}+\frac{\partial T\omega}{\partial t}=\frac{\partial}{\partial \sigma}\left[\frac{K_H}{D}\frac{\partial T}{\partial \sigma}\right]+F_T \quad ,(4)$$

$$\frac{\partial SD}{\partial t}+\frac{\partial SuD}{\partial x}+\frac{\partial SvD}{\partial t}+\frac{\partial S\omega}{\partial t}=\frac{\partial}{\partial \sigma}\left[\frac{K_H}{D}\frac{\partial S}{\partial \sigma}\right]+F_S \quad ,(5)$$

The conservation equations for heat and salt are: where T is the temperature, S is the salinity, K_H is a coefficient of the vertical turbulent exchange of heat and salt, and F_T and F_S are the components of the horizontal diffusion of heat and salt.

The equation of state is of a modified UNESCO form (MELLOR, 1991).

The processes having a spatial scale smaller than the grid mesh size are parameterised in terms of horizontal diffusion, as described by MELLOR and BLUMBERG (1985):

$$F_x=\frac{\partial}{\partial x}\left(2A_M H\frac{\partial u}{\partial x}\right)+\frac{\partial}{\partial y}\left[A_M H\left(\frac{\partial u}{\partial y}+\frac{\partial v}{\partial x}\right)\right] , (6)$$

$$F_y=\frac{\partial}{\partial y}\left(2A_M H\frac{\partial v}{\partial y}\right)+\frac{\partial}{\partial x}\left[A_M H\left(\frac{\partial u}{\partial y}+\frac{\partial v}{\partial x}\right)\right] , (7)$$

$$F_{T,S}=\frac{\partial}{\partial x}A_H H\frac{\partial(T,S)}{\partial x}+\frac{\partial}{\partial y}A_H H\frac{\partial(T,S)}{\partial y} . (8)$$

Coefficients A_M and A_H are functions of the grid mesh size and velocity gradients:

$$A_M=A_H=C\Delta x\Delta y\frac{1}{2}\left|\nabla\vec{V}+\left(\nabla\vec{V}\right)^T\right| \quad , (9)$$

with:

$$\left| \nabla \gamma + \left(\nabla \gamma\right)^{T} \right| = \left[\left(\frac{\partial u}{\partial x}\right)^{2} + \frac{\left(\frac{\partial v}{\partial x} + \frac{\partial u}{\partial y}\right)^{2}}{2} + \left(\frac{\partial v}{\partial y}\right)^{2} \right]^{1/2}$$

Values of C are usually between 0.1 and 0.2, and with fine enough horizontal resolution C can be zero (OEY et al., 1985 a, b, c).

The vertical turbulent exchange coefficients K_M and K_H are obtained from the second-order turbulence closure model 'Level 2 1/2' (MELLOR and YAMADA, 1982). The turbulence closure model is based on equations for turbulent kinetic energy ($q^2/2$) and turbulent macroscale (l):

$$\frac{\partial q^2 D}{\partial t} + \frac{\partial uq^2 D}{\partial x} + \frac{\partial vq^2 D}{\partial y} + \frac{\partial \omega q^2}{\partial \sigma} =$$

$$= \frac{\partial}{\partial \sigma}\left[\frac{K_q}{D}\frac{\partial q^2}{\partial \sigma}\right] + \frac{2K_M}{D}\left[\left(\frac{\partial u}{\partial \sigma}\right)^2 + \left(\frac{\partial v}{\partial \sigma}\right)^2\right] + \quad ,(10)$$

$$+ \frac{2g}{\rho_o} K_H \frac{\partial \widetilde{\rho}}{\partial \sigma} - \frac{2Dq^3}{B_1 l} + F_q$$

$$\frac{\partial q^2 D}{\partial t} + \frac{\partial uq^2 D}{\partial x} + \frac{\partial vq^2 D}{\partial y} + \frac{\partial \omega q^2}{\partial \sigma} =$$

$$= \frac{\partial}{\partial \sigma}\left[\frac{K_q}{D}\frac{\partial q^2}{\partial \sigma}\right] + \frac{2K_M}{D}\left[\left(\frac{\partial u}{\partial \sigma}\right)^2 + \left(\frac{\partial v}{\partial \sigma}\right)^2\right] + \quad ,(11)$$

$$+ \frac{2g}{\rho_o} K_H \frac{\partial \widetilde{\rho}}{\partial \sigma} - \frac{2Dq^3}{B_1 l} + F_q$$

where E_1, E_2 and B_1 are empirical constants (MELLOR and YAMADA, 1982). Functions $\widetilde{W}$ and $\frac{\partial \widetilde{\rho}}{\partial \sigma}$ are defined as follows:

$$\widetilde{W} = 1 + E_2\left(\frac{l}{kL}\right), L^{-1} = \left(\eta - z\right)^{-1} + \left(H - z\right)^{-1} (12)$$

$$\frac{\partial \widetilde{\rho}}{\partial \sigma} \equiv \frac{\partial \rho}{\partial \sigma} - c_s^{-2}\frac{\partial p}{\partial \sigma} \qquad (13)$$

where c_s is the speed of sound.

The terms F_q and F_l represent horizontal mixing and are parameterised in the same way

as the corresponding terms for temperature and salinity from equations (4) and (5).

When details of the closure model are rather involved, expressions for vertical exchange coefficients are reduced to (MELLOR and YAMADA, 1982):

$$K_M = lqS_M \qquad (14)$$

$$K_H = lqS_H \qquad (15)$$

$$K_q = lqS_q \qquad (16)$$

The stability functions S_M, S_H and S_q are obtained from analytical assumptions of the turbulence closure model. They are the algebraic function of $\partial u/\partial z$, $\partial v/\partial z$, $g\rho_o^{-1}(\partial \rho/\partial z)$, q and l and are given by:

$$S_M\left[6A_1A_2G_M\right] +$$
$$+ S_H\left[1 - 2A_2B_2G_H - 12A_1A_2G_H\right] = A_2 \qquad (17)$$

$$S_M\left[1 + 6A_1^2G_M - 9A_1A_2G_H\right] -$$
$$- S_H\left[12A_1^2G_H + 9A_1A_2G_H\right] = A_1(1 - 3C_1) \qquad (18)$$

$$S_q = 0.20 \qquad (19)$$

and:

$$G_M = \frac{l^2}{Dq^2}\left[\left(\frac{\partial u}{\partial \sigma}\right)^2 + \left(\frac{\partial v}{\partial \sigma}\right)^2\right]^{1/2} \qquad (20)$$

$$G_H = \frac{l^2}{Dq^q}\frac{g}{\rho_o}\frac{\partial \rho}{\partial \sigma} \qquad (21)$$

On the basis of laboratory experiments, the empirical constants are (MELLOR and YAMADA, 1982):

$$(A_1, A_2, B_1, B_2, C_1) =$$
$$= (0.92, 0.74, 16.6, 10.1, 0.08) \qquad (22)$$
and
$$(E_1, E_2) = (1.8, 1.33). \qquad (23)$$

The boundary condition at the sea surface ($\sigma = 0$) for the momentum equation is given by:

$$\frac{\rho_0 K_M}{D}\left(\frac{\partial u}{\partial \sigma}, \frac{\partial v}{\partial \sigma}\right) = (\tau_{ox}, \tau_{oy}) \qquad (24)$$

with

$$\tau_{ox} = C_D \rho_a u_a \sqrt{u_a^2 + v_a^2} \qquad (25)$$

$$\tau_{oy} = C_D \rho_a v_a \sqrt{u_a^2 + v_a^2} \qquad (26)$$

and

$$C_D = 10^{-3}\left(1 + 0.07\sqrt{u_a^2 + v_a^2}\right) \qquad (27)$$

where ρ_a is the air density, and u_a and v_a are the wind components in the x and y directions (DEACON and WEBB, 1962), for the continuity equation:

$$\omega(0) = 0 \qquad (28)$$

for turbulent kinetic energy q^2:

$$q^2 = B_1^{2/3} u_{\tau s}^2 \qquad (29)$$

for turbulent macroscale l:

$$q^2 l = 0 \qquad (30)$$

where $u_{\tau s}$ is the friction velocity at the sea surface and $B_1^{2/3}$ is empirical constant obtained from the laboratory experiments.

At the sidewalls there are no normal temperature and salinity gradients and there are no advective and diffusive fluxes across these boundaries.

At the bottom ($\sigma = -1$) the momentum equation is replaced by:

$$\frac{\rho_0 K_M}{D}\left(\frac{\partial u}{\partial \sigma}, \frac{\partial v}{\partial \sigma}\right) = (\tau_{bx}, \tau_{by}) \qquad (31)$$

the continuity equation by:

$$\omega(-1) = 0 \qquad (32)$$

the equation for the turbulent kinetic energy by:

$$q^2 = B_1^{2/3} u_{\tau b}^2 \qquad (33)$$

and, finally, the equation for the turbulent macroscale by:

$$q^2 l = 0 \qquad (34)$$

where $u_{\tau b}$ is the friction velocity connected to the bottom frictional stress (τ_{bx}, τ_{by}). The bottom stress is determined by matching velocities with the logarithmic law of the wall, at least at sufficiently shallow water:

$$\tau_{by} = \rho_o C_D |V_b| v_b \qquad (35)$$

with the drag coefficient given by:

$$C_D = \frac{\kappa^2}{[\ln(1+\sigma_{kb-1})H/z_o]^2} \qquad (36)$$

where v_b is the bottom velocity, k is the Von KARMAN constant, and z_o is the bottom roughness. According to WEATHERLY and MARTIN (1978), $z_o = 1$ cm. In those instances where the bottom boundary layer is not well resolved, C_D is taken to be equal to 2.5×10^{-3}. Inside the model code higher value between 2.5×10^{-3} and (36) expression is selected.

The heat and moisture fluxes are assumed to be zero at the surface and at the bottom of the Kaštela Bay, since we are interested in the numerical studies of the wind-induced currents and their dependence on the topography and on the vertical distribution of density. In the future, processes of heat and moisture exchange at the atmosphere-sea interface should be taken into account.

Open boundary conditions for the scalar variables, temperature and salinity, demand only nonlinear, advective parts of the equations. Temperature and salinity at the inflowing boundaries are provided from empirical data, whereas the following expression is used for outflowing boundaries:

$$\frac{\partial}{\partial t}(T, S) + u_n \frac{\partial}{\partial n}(T, S) = 0 \qquad (37)$$

where n is the coordinate normal to the open boundary and u_n is the velocity component normal to the open boundary. Turbulent kinetic energy and the turbulent macroscale are calculated at the open boundary by neglecting non-

linear terms. The tangential velocity component is assumed to be zero. The normal velocity component is provided from the radiation condition:

$$\frac{\partial v}{\partial t} + c_i \frac{\partial v}{\partial y} = 0 \qquad (38)$$

where c_i is the phase speed of gravitational waves.

The hydrodynamic equations are solved in the ARAKAWA C-grid. The central differencing is used in space and time, with an explicit time scheme in the horizontal direction and an implicit time scheme for the vertical diffusion. Due to computer efficiency, a mode-splitting technique is used (SIMONS, 1974). The baroclinic and barotropic modes have different stability conditions, and different time steps can be used for each of them.